Dear reviewer,

Thanks very much for taking your time to review this manuscript. We really appreciate all your comments and suggestions! We did our best to respond to each comment and revise the original manuscript. Details are listed as follows.

The manuscript seeks to investigate the impact of multiscale turbulence structures within the urban canopy layer (UCL) of a basin city on haze pollution processes, using field observations from Lanzhou, China. It identifies a typical daily cycle of $PM_{2.5}$ concentration variations, influenced by small-scale turbulence, sub-mesoscale motions, and anthropogenic heat sources. The study employs turbulence decomposition techniques, quadrant analysis, and spectral analysis to understand the complex interactions between turbulence and haze pollution, with implications for improving urban air pollution forecasting. The authors highlight how turbulent eddies with timescales under 15 minutes contribute to pollutant dispersion, while coherent structures such as thermal plumes influence pollutant transport. Specifically, they conclude that small-scale turbulent eddies enhance pollutant dispersion and sub-mesoscale motions contribute to turbulence intermittency. While the manuscript seeks to address a complex and relevant issue, major concerns have been identified as discussed in the general and specific points below:

Response: Thank you for your positive and constructive comments to our study. We were greatly encouraged. We fully agree with your helpful suggestions and have thoroughly incorporated them into our study, making some supplements to the content. These changes helped to enhance the reliability and objectivity of our study conclusions. Details are listed as follows.

General comments：

1. Writing: The writing is at times confusing and/or contradictory. A thorough editing, looking for typos and unclear sentences, should be done.

Response: Thank you very much for your careful reading and checks. We sincerely apologize for the confusing and contradictory in our writing. We have fully acknowledged these problems and carefully reviewed them to prevent their recurrence.

Further details can be found in our replies to the specific comments below.

2. Evidence in support of conclusions: The scientific claims and conclusions are not well supported by the evidence provided in the results, as detailed in the specific comments below. A major concern is that the study relies on observational data from a single monitoring station, which may not adequately capture spatial variations in turbulence and pollution dynamics across the city. Given only hourly pollution data are used in the analysis, could other sensors from the city included to analyze spatio-temporal coherence of the pollution? This limitation makes it impossible to determine whether the observed features are representative of the entire urban area, both in terms of pollution and meteorological/turbulence dynamics. This is a critical issue, given the study's objective of assessing the influence of multiscale drivers on urban pollution and haze events. For instance, the analysis lacks sufficient evidence to draw definitive conclusions about the impact of sub-mesoscale motions on pollutant dispersion.

Response: Thank you so much for your valuable comments and suggestions, your suggestions are very helpful to our study.

We fully agree with your point that "observational data from a single monitoring station may not adequately capture spatial variations in turbulence and pollution dynamics across the city". And we also sincerely appreciate your suggestion that " other sensors from the city included to analyze spatio-temporal coherence of the pollution". Therefore, we further analyze the spatio-temporal characteristics of the haze pollution pattern in Lanzhou Basin city by using the data from China National Environmental Monitoring Center (available at https://www.cnemc.cn/sssj/), which were collected from in January 2021 and December 2023 to February 2024.

In Lanzhou Basin city, there are also 4 state-controlled monitoring sites, which were shown Figure 1. These sites include LLBG (36.10°N,103.63°E), ZGYY (36.08°N,103.71°E), SWZPS (36.07°N,103.84°E), TLSJY (36.05°N,103.83°E). The environmental conditions around the monitoring sites were relatively stable to avoid other effects such as torrential flood and mud-rock flows (Zhao et al., 2017). These

stations utilize automated monitoring equipment to obtain real-time concentration data of air pollutants (including $PM_{2.5}$) with a time resolution of 1 hour. Firstly, we conducted a station average analysis of $PM_{2.5}$ concentration data from 4 state-controlled monitoring sites in January 2021. Then, we compared the results with those from Lanzhou atmospheric components monitoring superstation (LACMS), which served as the observation station in our original study, and found that their pattern characteristics were consistent. Furthermore, we have analyzed the $PM_{2.5}$ concentration data from subsequent observations conducted from December 2023 to February 2024, and the results have also shown consistency (see Figure 2). In summary, the spatial and temporal characteristics of Lanzhou Basin city from January 2021 and December 2023 to February 2024 exhibit consistency. During the haze pollution periods, the pattern characteristics of $PM_{2.5}$ concentrations were observed as follows: an increase from 08:00-13:00, a decline from 14:00-18:00, a subsequent rise from 19:00-21:00, and a decrease again from 22:00-07:00 the next day. Thank you again for your constructive suggestions, which increase the reliability of our study conclusions on the spatio-temporal characteristics of haze pollution pattern.

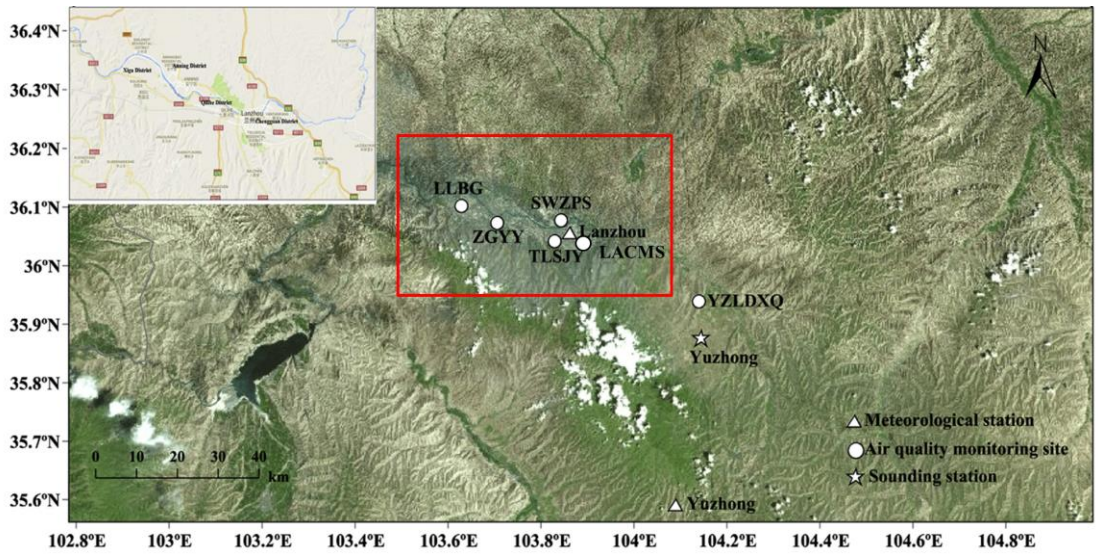

Figure 1. The monitoring sites of air pollutants in urban and rural areas of Lanzhou, Lanzhou atmospheric components monitoring superstation (LACMS; the observation station in our original study) is also included, and the observation stations in the urban area are shown in the red box. (Cited from Zhao et al., 2017, Figure 1)

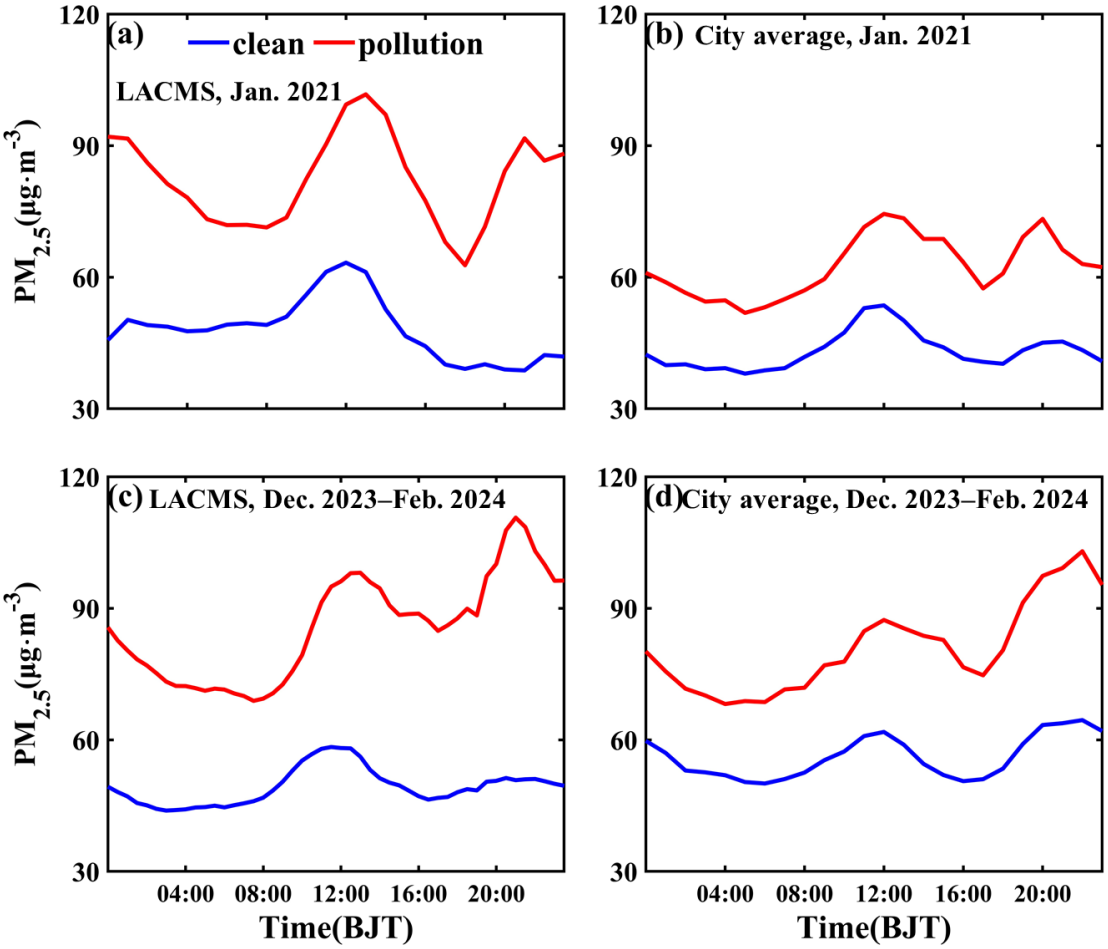

Figure 2. The mean diurnal variation of concentrations of $PM_{2.5}$, (a) is from LACMS in January 2021, (b) is from City average in January 2021, (c) is from LACMS in December 2023 to February 2024, and (d) is from City average in December 2023 to February 2024. City average refers to the data obtained from a station average across 4 state-controlled monitoring sites.

We study the characteristics of the turbulence structures in the UCL of basin. The UCL height is defined as the average height of rough elements, and the UCL is the most drastically affected by pollution sources emissions from surface and anthropogenic activities (Oke et al., 2017). The underlying surface of urban is mainly composed of rough elements such as buildings and trees. The turbulence data observed by the eddy covariance system, affected by the highly inhomogeneous distribution of rough elements, primarily reflect the region dominated by the characteristics of roughness elements around the site. This scale is generally considered as the street scale (see Figure 3). Furthermore, we used a flux footprint model (Kljun et al., 2015) to determine the spatial representativeness of the observed eddy covariance systems on the complex underlying surfaces of urbans. It can be seen from Figure 4 that the fluxes contribution

in the northeast direction of the observation station is the highest, while the contribution to the south is minimal due to the dense presence of buildings in that area. The maximum range of fluxes contributions can reach up to 0.36 km^2. Although rough elements in the UCL exhibit varying distribution characteristics across different regions, their presence exerts certain common effects on dynamic and thermal turbulence. For example, significant roughness caused by the canopy and its geometry directly influences the flow fields (Russell et al., 2016; Zou et al., 2017; Shi et al., 2023), and the anthropogenic heat and urban canopy storage heat will continuously affect the regional atmosphere (Li et al., 2021). Existing studies examining the correlation between turbulence and air pollution in urban area are mainly based on single monitoring station (Shi et al., 2023; Román-Cascón et al., 2023). Unfortunately, due to a lack of dense turbulence observations in Lanzhou city at present, we are unable to obtain additional turbulence data from that location. In fact, dense turbulence observations are not that sufficient in any city. However, we can provide extended observation records from our monitoring site, which further substantiate the generality of our results, just as you suggested. For specific conclusions regarding this matter, please refer to the next reply.

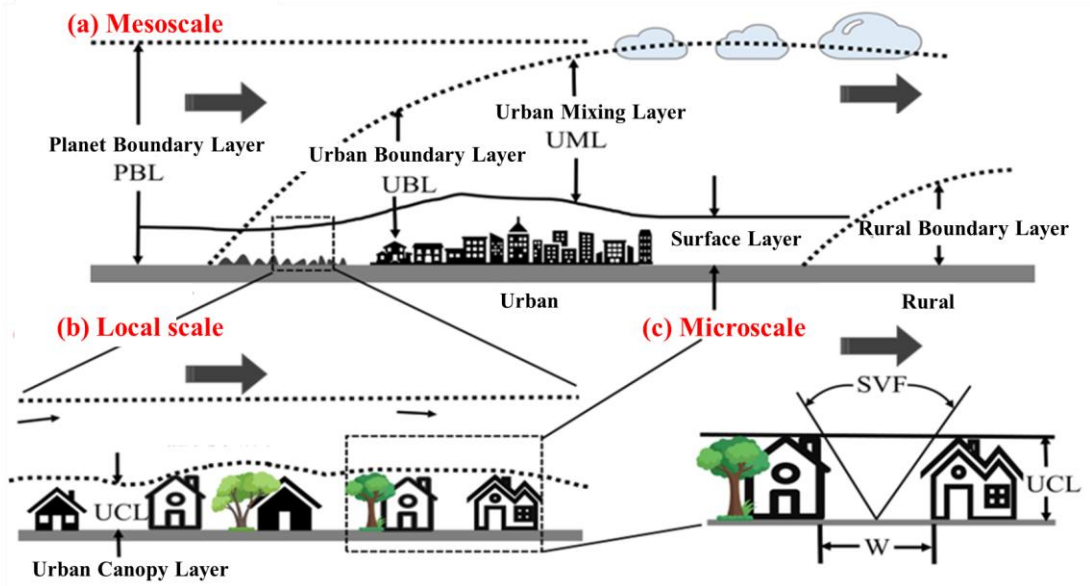

Figure 3. Sketch of the urban boundary layer structure indicating the various (sub)layers and their names, SVF and W stand for sky view factor and the width of the street canyons. (Cited and revised from Rotach et al., 2005, Figure 1)

Figure 4. The flux footprint map calculated by the Flux Print Prediction model developed by Kljun et al. illustrates the contributions of flux, represented by red circles. These contributions range from 10% to 90%, increasing in increments of 10%, as observed in January 2021.

We are sorry for the unclear description of our research conclusions on the impact of sub-mesoscale motions on pollutant diffusion. Affected by the highly inhomogeneous distribution of rough elements within the UCL, the collected high-frequency turbulent signals are severely contaminated by sub-mesoscale motions (Anfossi et al., 2005; Vickers and Mahrt, 2006; Mahrt, 2014). Mahrt (2014) defined sub-mesoscale motions as "motions between the primary turbulent eddies and smallest mesoscale motions". Sub-mesoscale motions include drainage flows, horizontal meandering, internal gravity waves, "dirty waves", among others. Moreover, our observations have found the non-turbulent feature of "dirty waves" in the UCL. It can be seen from Figure 5 that original u′, v′, and w′ are all characterized by distinct wavelike signals. The amplitude and period of waves vary between cycles, which is referred to as "dirty waves" (Mahrt 2014; Cava et al. 2015). The separated sub-mesoscale signals of u′, v′, and w′ (i.e., black lines in Figure 5a–c) follow the "dirty waves" well, which means the sub-mesoscale motions represent as "dirty waves" in the UCL. This form of expression reflects the characteristics of the complex underlying surface.

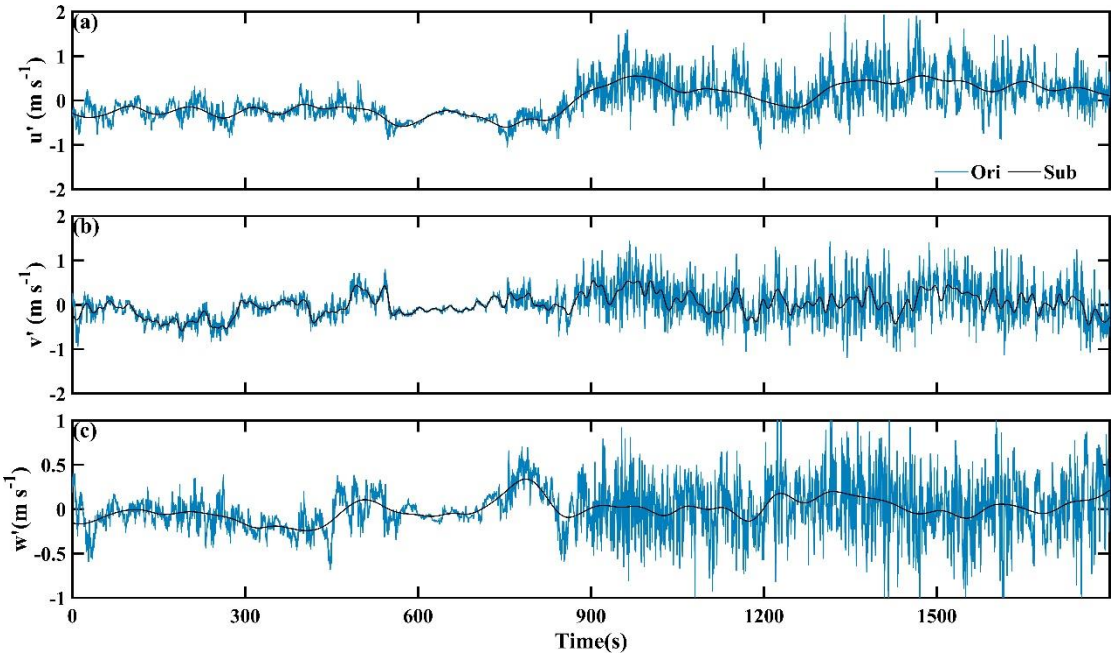

Figure 5. Time series of original (a) u′, (b) v′, and (c) w′ for the selected 30-min segment in the UCL of basin. The black solid lines represent the fluctuations induced by sub-mesoscale motions.

Our findings indicate that during nighttime, although turbulence intensity remained still weak, sub-mesoscale motions drove turbulence intermittency events, facilitating kinetic energy transition from sub-mesoscale to turbulent motions. These short-term turbulence bursts led to a reduction in $PM_{2.5}$ concentrations. Additionally, sub-mesoscale motions formed organized coherent structures, also further contributing to the decrease in $PM_{2.5}$ concentrations. The period, during 00:00-07:00 on January 14, 2021, was in turbulent quiescent period with high turbulence intermittency intensity and lower wind speeds (see Figure 6), yet it corresponded to a decrease of $PM_{2.5}$ concentration. We further utilized the quadrantal analysis to discuss that the organized structure formed by the larger-scale sub-mesoscale motions played a positive role in the dissipation of $PM_{2.5}$.

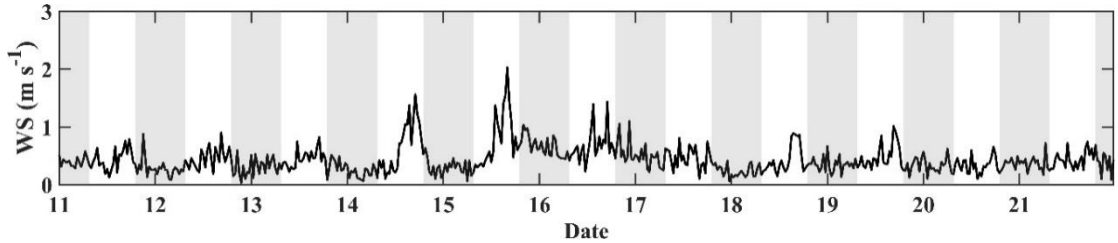

Figure 6. Time series of horizontal wind speed (WS) from January 11 to 21, 2021. The gray shading represents night between 19:00 and 07:00 the following day.

We have realized that the original analysis lacks sufficient evidence to draw definitive conclusions about the impact of sub-mesoscale motions on pollutant dispersion. As pointed out by the first reviewer, we did not clearly articulate the basis for partitioning between sub-mesoscale motions and turbulent motions and the definition of the spectral gaps. To solve this problem, we have made corresponding substantial revisions in both the introduction and methodology sections. Specific comments No. 12 to 16 below explicitly address these issues related to the sub-mesoscale motions. We also have made appropriate corrections in response to these points; further details can be found in our replies to specific comments No. 12 to 16 below.

3. Generalizability of findings: Related to point 2, there are concerns about the generalizability of the findings to other urban areas or time periods. The study focuses solely on Lanzhou, making it difficult to extend its conclusions to cities with different topographies and climates. If data from other locations are not available, a longer time series of events should be analyzed to ensure statistically robust conclusions.

Response: Thank you so much for your helpful comments and suggestions. We fully agree with your suggestions and have thoroughly incorporated them into our study, making some supplements to the content. The details are as follows.

As mentioned in the second response above, our observation platform is located in the UCL, where we concentrate on urban microscale meteorological research. Turbulence data observed in the UCL are significantly affected by sub-mesoscale motions, resulting in highly complex turbulence structures. Furthermore, the spatial representation of observed data is mainly on the street scale. Regarding your suggestion about extending the conclusions drawn from the UCL of the Lanzhou Basin to other cities with different topographies and climates, we would like to note that turbulence structures in the urban boundary layer and their impacts on haze pollution events can vary significantly across cities. The findings of this study regarding pollution process patterns and the impacts of multi-scale turbulence structures are characteristic of the

UCL in basin cities and exhibit distinct features that differentiate them from those in plain cities. We compared our research findings from the semi-arid region of Lanzhou Basin city with those from other cities situated in different topographical and climatic conditions, such as Beijing and Tianjin, which are located in the temperate monsoon climate zone. As illustrated in Figure 7, Figure 8 and Figure 9, the haze pollution patterns observed in the North China Plain differ significantly from those found within the UCL of Lanzhou Basin. Notably, there is no distinct diurnal variation characteristic. Figure 9a shows the time series of surface $PM_{2.5}$ concentration of Beijing city from 3 November 2017 to 15 January 2018, the $PM_{2.5}$ concentration variation patterns show distinct ramp-like structures. That is to say, the $PM_{2.5}$ accumulated slowly from the low level to the high value in approximately 3–4 days, and then decreased rapidly back to the low concentration. The unique topography of basin more prone to inducing cold pool events that will result in the formation of stable boundary layer (Lareau et al., 2013). However, simultaneously, behaviors such as urban heating increase anthropogenic heat sources and promote the development of an unstable boundary layer. These two opposite processes will result in different atmospheric turbulence structures, influencing haze pollution events distinctly, and resulting a distinctive pollution pattern in the UCL of Lanzhou Basin.

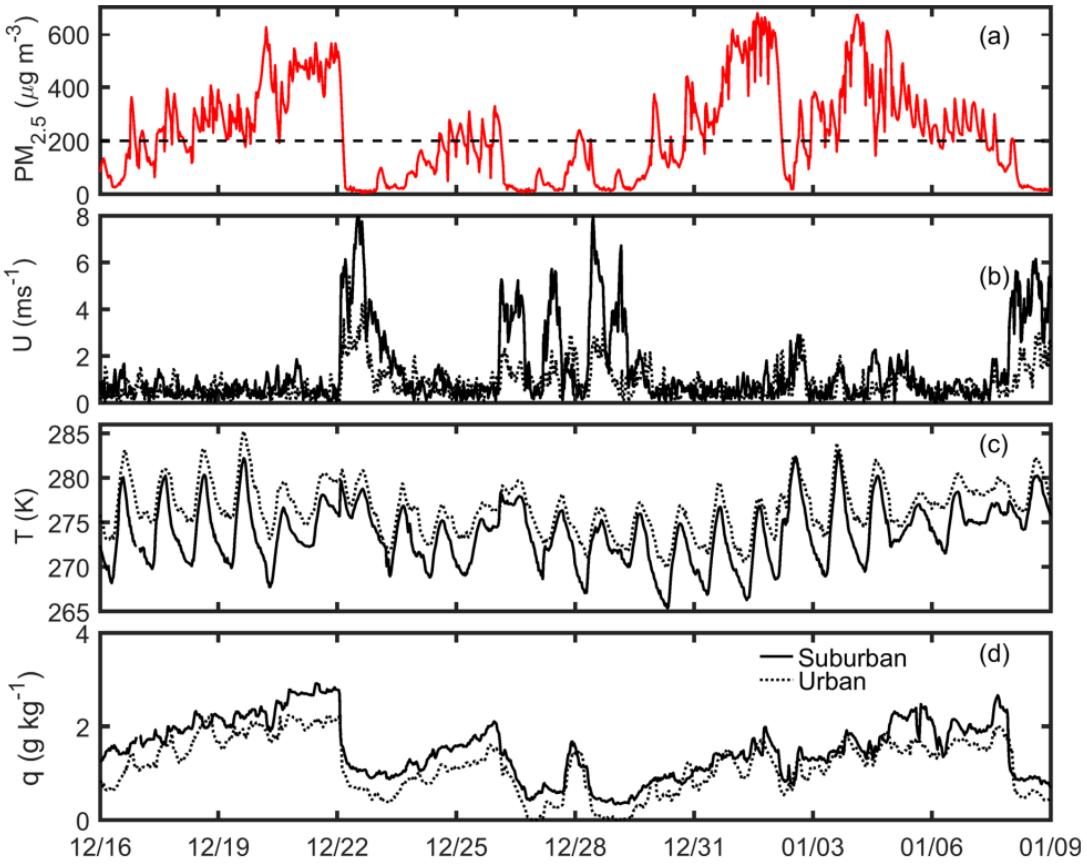

Figure 7. The $PM_{2.5}$ mass concentration (a), horizontal wind speed (b), virtual temperature (c), and water-vapour mixing ratio (d) from 16 December 2016 to 8 January 2017. The black solid line represents data from the suburbs of Beijing (flat terrain), and the black dotted line represents data from the Peking University site (urban landscape). (Cited from Ren et al., 2019a, Figure 3, underlying surface of Beijing city)

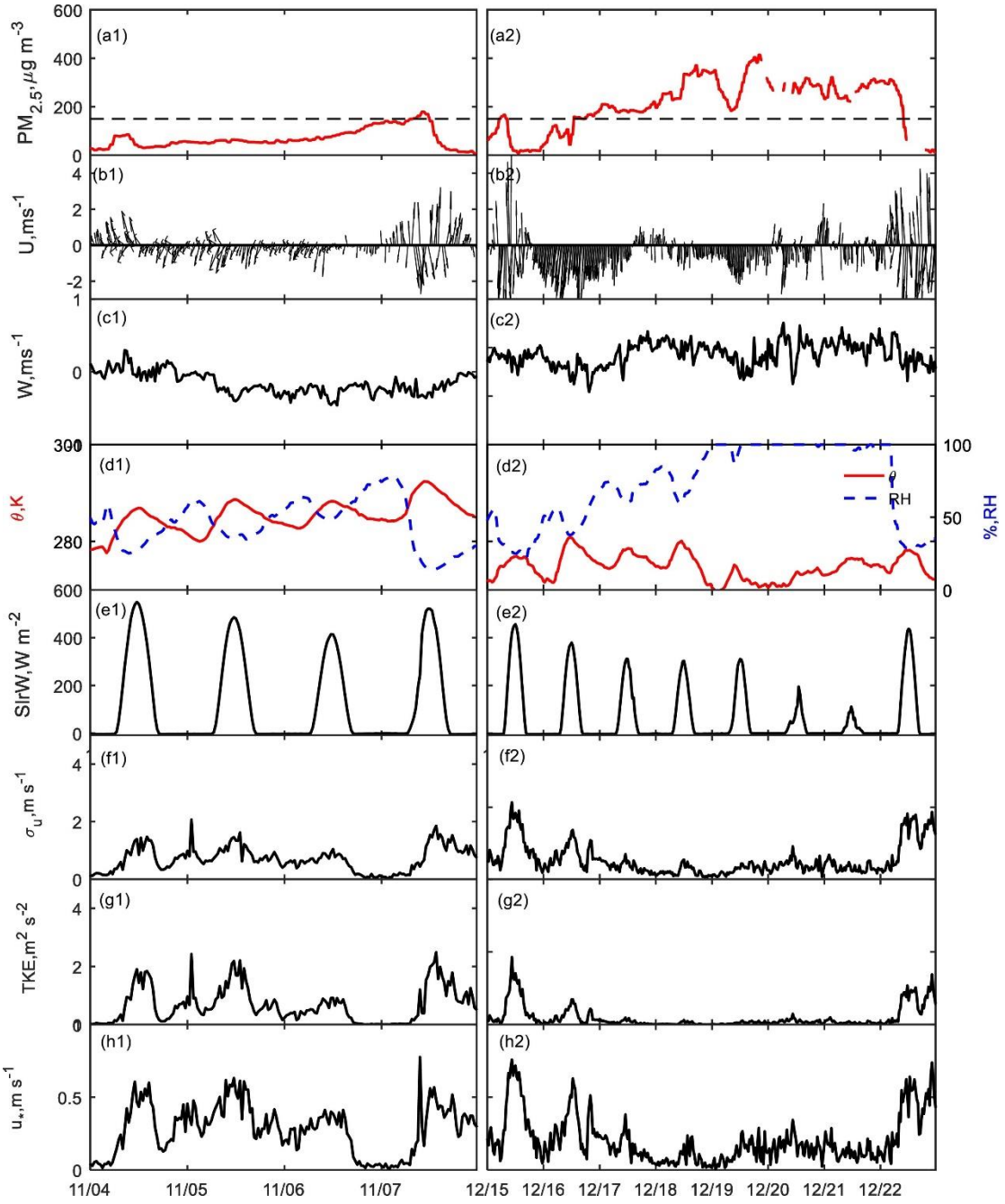

Figure 8. Time series of the $PM_{2.5}$ mass concentration (a1-a2), horizontal wind vector (b1-b2), vertical wind speed (c1-c2), potential temperature and relative humidity (d1-d2), solar shortwave radiation (e1-e2), σ_u (f1-f2), TKE (g1-g2) and u_* (h1-h2). (Cited from Ren et al., 2019b, Figure 6, underlying surface of Tianjin city)

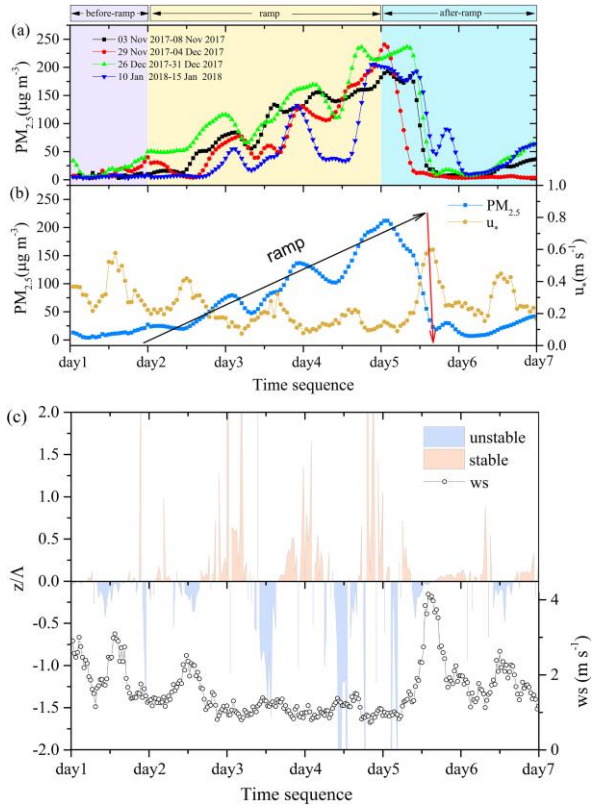

Figure 9. (a) Time series of surface $PM_{2.5}$ concentration of four pollution processes from 3 to 8 November 2017, 29 November to 4 December 2017, 26 to 31 December 2017, and 10 to 15 January 2018; (b) averaged concentration of $PM_{2.5}$ of the four pollution processes; (c) Time series of the averaged stability parameter and wind speed of the four pollution processes observed at 15 m on the Beijing 325-m tower. (Cited from Shi et al., 2020, Figure 1, underlying surface of Beijing city)

Thank you so much for your suggestion that this study needs to analyze longer time series of events to improve the generalizability of the conclusions. By using the turbulence and $PM_{2.5}$ concentration observation data of LACMS from December 2023 to January 2024, we further analyzed the characteristics of haze pollution pattern and turbulence structures in the UCL of Lanzhou Basin in winter (see Figure 2c and Figure 10). We can see that the subsequent observations were similar to those of January 2021 (see Figure 11). The turbulent kinetic energy TKE, friction velocity u_*, sensible heat flux H and stability (z-d)/L have obvious diurnal variation characteristics. On the whole, the TKE and u_* in the cleaning period were higher than that in the pollution period (see Figure 10b and 10c), but the sensible heat flux (H) was larger and the instability was higher during the pollution period (see Figure 10e). In addition, we also found that

the turbulent structure characteristics in the UCL of basin differ significantly from those in plain cities (Ren et al., 2019a; Wang et al., 2020). Specifically, the sensible heat flux was reduced and the atmospheric stratification was more stable during haze pollution periods (see Figure 12a and 12e). However, the observations of our studies indicated that the sensible heat flux was greater and the atmospheric instability was stronger during haze pollution periods, which may be attributed to the stronger influence of human activities.

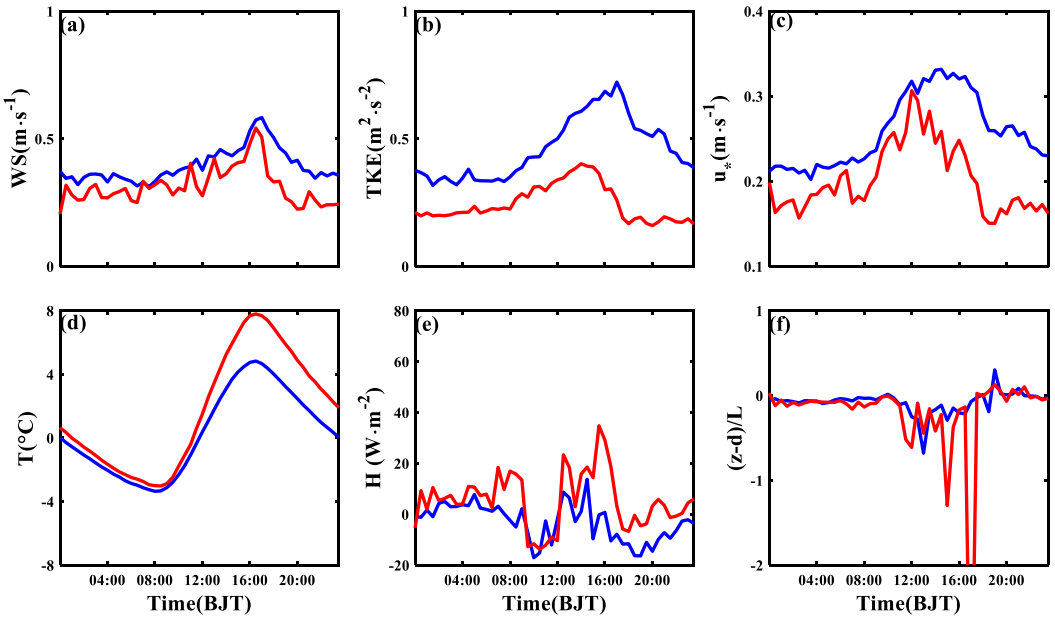

Figure 10. The mean diurnal variation of (a) horizontal wind speed (WS), (b) turbulent kinetic energy (TKE), (c) friction velocity (u_*), (d) temperature (T), (e) sensible heat flux (H), and (f) stability parameter ((z-d)/L) under different conditions from LACMS during December 2023 to January 2024. Solid blue and red lines indicate clean and pollution periods, respectively.

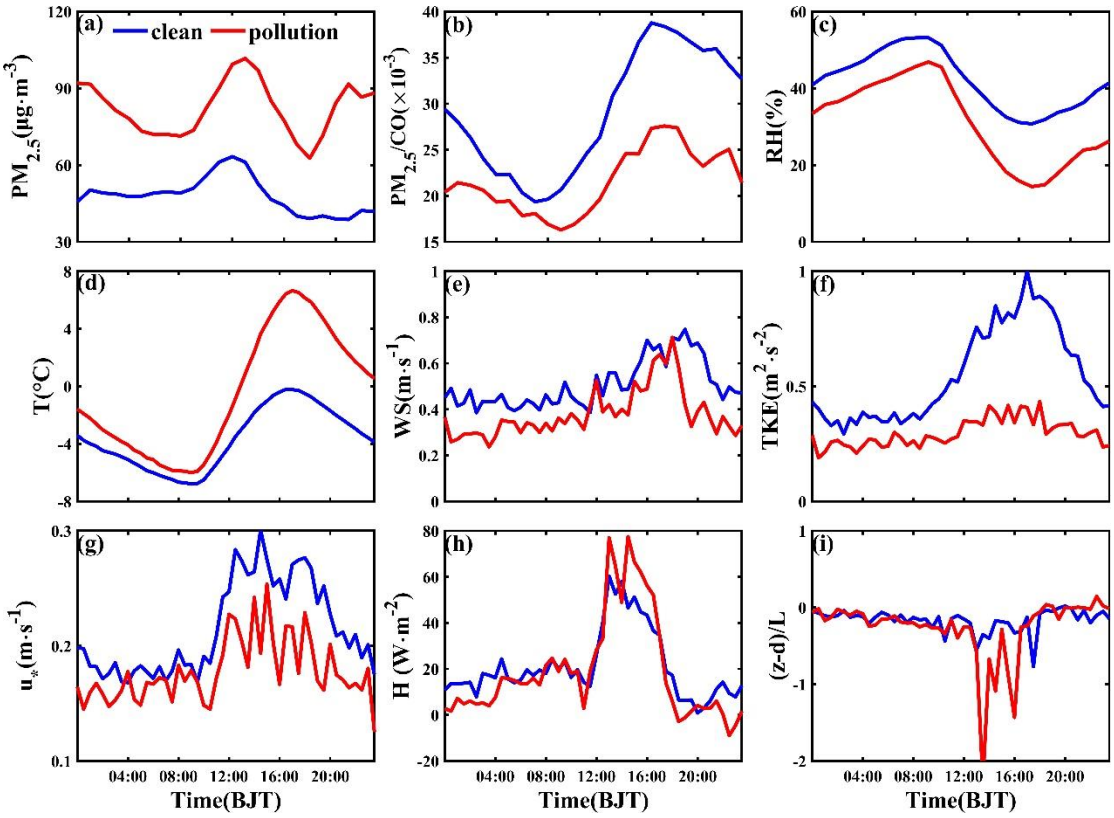

Figure 11. The mean diurnal variation of (a) concentrations of $PM_{2.5}$, (b) $PM_{2.5}$/CO, (c) relative humidity (RH), (d) temperature (T), (e) horizontal wind speed (WS), (f) turbulent kinetic energy (TKE), (g) friction velocity (u_*), (h) sensible heat flux (H), and (i) stability parameter ((z-d)/L) under different conditions from LACMS in January 2021. Solid blue and red lines indicate clean and pollution periods, respectively. (From original manuscript Figure 2)

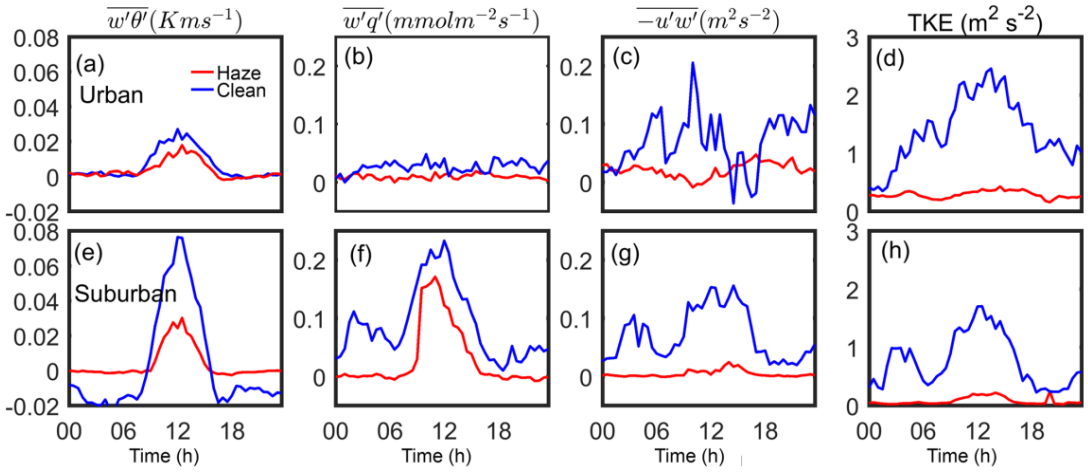

Figure 12. Diurnal variations in the mean vertical heat flux (a), vertical water-vapour flux (b), momentum flux (c), and TKE (d) under polluted weather (red solid line) and clear weather (blue solid line) conditions over the urban site. Diurnal variations in these variables over the suburban site are shown in (e), (f), (g), and (h). (Cited from Ren et al., 2019a, Figure 11)

Finally, thanks again for your valuable comments and suggestions. We would like

to standardize the expression and supplement the longer time series analysis in the UCL of Lanzhou Basin city and comparative analysis with other cities in section 3.1. Which would help ensure that our study conclusions are more reliable and objective.

4. Methods: While the study provides a detailed observational analysis, its conclusions often rely on visual inspections of metrics and indicators derived from observational data, lacking robust statistical analyses or objective methods to distinguish specific dynamics and regimes. Additionally, the absence of a predictive modeling component limits the study's ability to test the influence of various turbulence structures under different conditions. Although the study highlights human activities as a primary driver of pollution events, it does not provide a detailed quantification of emissions in space or time, nor does it analyze their interaction with turbulence structures. It remains unclear whether the pollution is solely locally produced. A spatial emission map or pollution modeling would help clarify the sources, drivers, and relevant scales of these events.

Response: Thank you so much for your helpful comments and suggestions. We fully understand your concerns regarding the objectivity of the methods we employed. We sincerely apologize for the unclear presentation of our methodology in the introduction and methods sections. Therefore, we would like to introduce the methods and the parameters that we employed, the limitation and application of existing predictive modeling in the UCL, and source emission characteristics of Lanzhou Basin. The details are as follows.

(1) Classical turbulence statistical parameters

The turbulent statistics parameters such as turbulent kinetic energy (TKE), friction velocity (u_*), sensible heat flux (H), and the local Obukhov length (L) in our manuscript are widely used in the research of atmospheric turbulence (Stull, 1988; Kaimal & Finnigan, 1994). Their scientific validity and universality have been fully verified by decades of theoretical derivation, field observations and numerical simulations.

(2) The basis for distinguishing sub-mesoscale motions and turbulent motions

Distinct spectral gaps have been detected in energy spectra of turbulence quantities

in many studies with the help of different mathematical tools (Muschinski et al., 2004; Vickers and Mahrt, 2003). To decompose turbulent and sub-mesoscale parts in the observed fluctuations, spectral approaches are usually adopted, on the basis of the appearance of spectral gaps between turbulence and sub-mesoscale motions (Mahrt, 2007; Wei et al. 2017; Mahrt and Bouzeid, 2020). Common spectral analysis methods include wavelet analysis (Salmond 2005), multi-resolution decomposition (MRD; Vickers and Mahrt 2003; Acevedo et al. 2014) and Hilbert–Huang transform (HHT; Huang et al. 2008; Wei et al. 2017), the latter of which appears to be superior as it is fully data-driven. Ren et al. (2019a) developed an algorithm based on the HHT to separate and reconstruct sub-mesoscale and turbulent motions (SMT). The proposed algorithm looks for spectral gaps between large- (weather-scale) and small-scale (turbulence-scale) motions from the Hilbert spectra of observational data, based on which the algorithm subsequently reconstructs the turbulent motion series. In the second-order Hilbert spectra (see Figure 13), we can clearly observe the significant spectral gaps. The right sides of these spectral gaps aligned with the expectations of classical energy spectrum theory, whereas the left sides showed deviations from these expectations. Similarly, the study of Liu et al. (2023) also explored the application of spectral gaps in distinguishing sub-mesoscale motions from turbulent motions, as shown in Figure 14. Furthermore, Ren et al. (2023a) improved SMT algorithm from the perspective of dynamical spectral gap identification, thereby enhancing the accuracy of the identification of spectral gaps in turbulent fluctuation signals. SMT can help process high frequency pulsation data, any turbulent variable can be separated into two parts, that is, $s' = s'_{turb} + s'_{sub}$, represent turbulent motion and sub-mesoscale motions respectively.

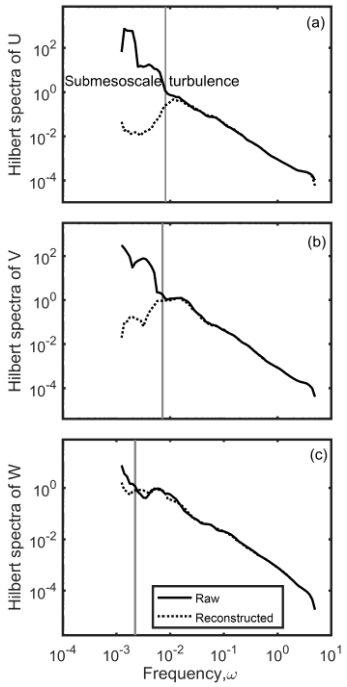

Figure 13. Second-order Hilbert spectra of three wind speed components U (a), V (b), and W (c) at 08:00 on 31 December 2016 at the suburban site. The black solid line indicates the spectra from the raw data, and the black dotted line indicates the spectra from the reconstructed data for pure turbulence. The solid gray lines indicate the position of the spectral gap. (Cited from Ren et al., 2019a, Figure 3)

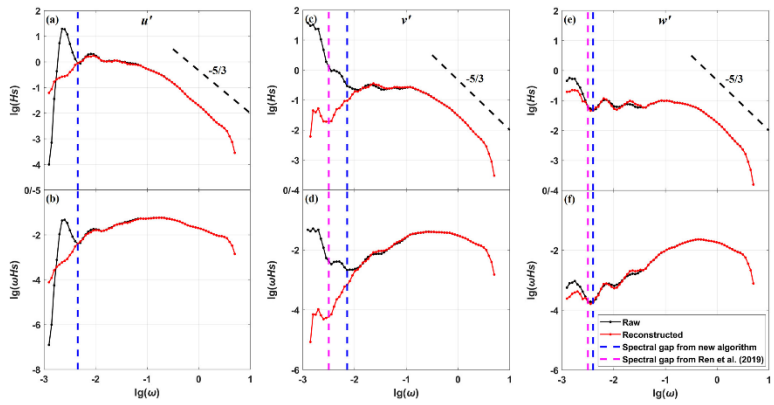

Figure 14. The second-order Hilbert spectra of three wind speed components u′ (a, b), v′ (c, d), and w′ (e, f) at 09:30 on 10 November 2019. The upper panels show the spectra of Hs, while the lower panels show the spectra of ωHs. The magenta and blue dashed lines indicate the locations of the spectral gap identified by Ren et al. (2019a) and our new algorithm, respectively. The solid black lines are the spectra from raw data, and the solid red lines represent the spectra from reconstructed data for pure turbulence according to the spectral gap identified by our new algorithm. (Cited from Liu et al., 2023, Figure 4)

(3) Quantitative characterization of turbulence intermittency

SMT can effectually quantitative characterization of sub-mesoscale motions, Ren

et al. (2019a, 2019b) proposed local intermittent strength of turbulence (LIST) and intermittency strength (IS) to quantitatively characterize turbulence intermittency from the perspectives of kinetic energy of turbulence and sub-mesoscale motions.

Furthermore, Ren et al. (2025) selected six methods from various perspectives to compare in this recent review. The different methods and indices show consistency in turbulent intermittency case and fully turbulent case. Furthermore, the indices (LIST and IS) can detect turbulence intermittency events and describe their characteristics, quiescent and burst periods. Additionally, the SMT method and LIST (IS) index have been applied to quantitative turbulence intermittency studies with different types of underlying surfaces, including homogeneous surfaces (Ren et al., 2023a), arid complex regions (Wei et al., 2021; Chang et al., 2024), desert hinterland (Zhang et al., 2024), polar regions (Liu et al., 2023), and urban areas (Ren et al., 2019a; Ju et al., 2022; Zhang et al., 2022).

(4) The limitation and application of prediction model in UCL

Based on the research methodologies employed, studies on urban surface layer can be broadly categorized into two primary approaches: numerical simulations and observational experimentations.

Traditional studies based on large eddy simulation (LES) have primarily focused on idealized atmospheric boundary layer conditions. In recent years, LES has been coupled with various microphysical processes, radiative processes, land surface models, chemical models, and has also been nested within mesoscale models. However, due to the complexity of boundary conditions setting, the existing LES methods still have some limitations in the numerical simulation of real urban underlying surfaces. Particularly in the numerical simulation of the UCL, accurately characterizing the disturbance effects of geometric features such as buildings on flow has emerged as a key scientific challenge. Moreover, the non-stationary and nonlinear turbulence phenomena investigated in this study, including sub-mesoscale motions and turbulence intermittency, are beyond the description scope of classical turbulence theories. For instance, Monin-Obukhov similarity theory is inapplicable (Roth and Oke, 1993; Roth, 2000; Zou et al., 2018), and the basic assumptions employed in the subgrid scales (SGS)

within LES, such as the statistical homogeneity of the horizontal dimensions and the applicability of Kolmogorov's theories to the subgrid range of eddies, are invalid (Shah and Bou-Zeid，2014). Therefore, widely used numerical models such as WRF-LES currently have limitations in simulating the complex multi-scale turbulence processes within the UCL.

Observation experiment is the most direct and effective method to understand the processes of atmospheric motions. They can directly obtain urban meteorological parameters and reveal the basic laws of atmospheric motions, providing a basis for numerical simulations and theoretical analyses. In the urban microscale meteorological research, a variety of experimental observation methods are used to analyze the wind and thermal environment as well as the flows in turbulent boundary layer, including field observations (Roth, 2000; Zou et al., 2017), reduced-scale physical modeling and outdoor measurements (Ahmad et al., 2005; Hang and Chen, 2022) and wind tunnel experiment (Raupach et al., 1980; Mo and Liu, 2023). Wind tunnel experiment is an effective means to study the physical mechanism behind atmospheric processes, which can be used to study the atmospheric motion in the near strata of cities under controlled external environment. However, due to the nature of simulation experiments, the external environment, such as solar radiation, large-scale atmospheric motion, and thermal inhomogeneity of the underlying surface, differs from real conditions. Consequently, accurately simulating urban near-surface laminar flow dynamics proves challenging, and only some physical processes can be analyzed. In contrast, field observation research has significant advantages in terms of objectivity and reliability. Compared with the flat natural underlying surfaces, there are relatively few studies on the turbulent structures in the UCL, and the mechanisms of their influence on haze pollution remain unclear. The studies of high-precision observations in the UCL of the basin are of great significance to improve the numerical simulations. How does the complicated multi-scale turbulent structures within the UCL of basin influence the occurrence and evolution of haze pollution events? This scientific question is of great significance for understanding the development and variation of the urban boundary layer as well as for improving urban air pollution forecasting.

However, your suggestion remains very important. We have attempted to incorporate the footprint model into the analysis of this study. Figure 4 and the related analysis will be included in the revised manuscript.

(5) Source emission characteristics

Existing relevant literatures have pointed out that the pollutants in the Lanzhou Basin city during winter were primarily local emission (Xu et al., 2016; Zhao et al., 2017). Higher concentration values associated with lower wind speeds can indicate local emissions, while higher concentration values corresponded to higher wind speeds can indicate regional transmission. To investigate whether the pollution is mainly locally produced, we analyzed the bivariate polar graph of the wind direction and wind speed changes of $PM_{2.5}$ in January 2021(see Figure 15). During both clean and polluted periods in our study, lower wind speeds were associated with higher $PM_{2.5}$ concentrations, which proved that pollutants were mainly locally produced. Furthermore, the vertical profiles of aerosols (see Figure 16) showed that the aerosol extinction coefficient decreased with increasing height, with its maximum value concentrated below 400 m near ground level. Due to the relatively enclosed topography of the basin, pollutants tended to accumulate at its bottom. This characteristic of vertical distribution further proved that pollutants in the Lanzhou Basin city are less influenced by regional transport and are mainly emitted or produced locally. Additionally, we also utilized the Hybrid Single-Particle Lagrangian Integrated Trajectory (HYSPLIT; Draxler and Rolph, 2003; Wang et al., 2014) model to illustrate the location of pollution source of Lanzhou Basin during January 2021. It can be seen from Figure 17 that the local air flow (C1) accounted for 52.96%, and the potential sources of $PM_{2.5}$ were mainly concentrated around Lanzhou Basin, which also indicated that Lanzhou Basin was greatly influenced by local pollution sources during winter.

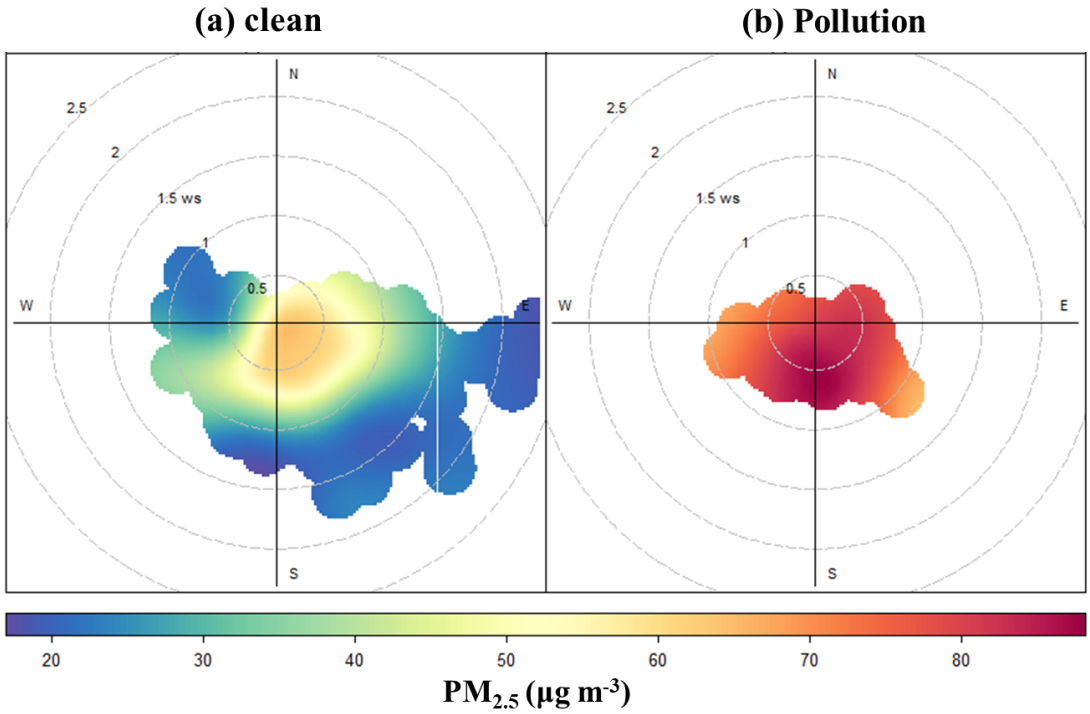

Figure 15. Bivariate polar plot of near-surface $PM_{2.5}$ concentrations (color) as a function of wind speed (distance from the center) and wind direction under clean and polluted conditions in January 2021.

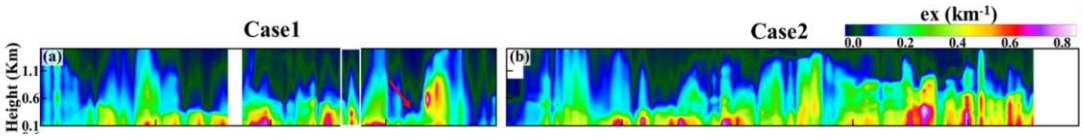

Figure 16. Time series of aerosol extinction coefficient profiles from Case 1 (January 11–14, 2021) and Case 2 (January 17–21, 2021). (From original manuscript Figure 5)

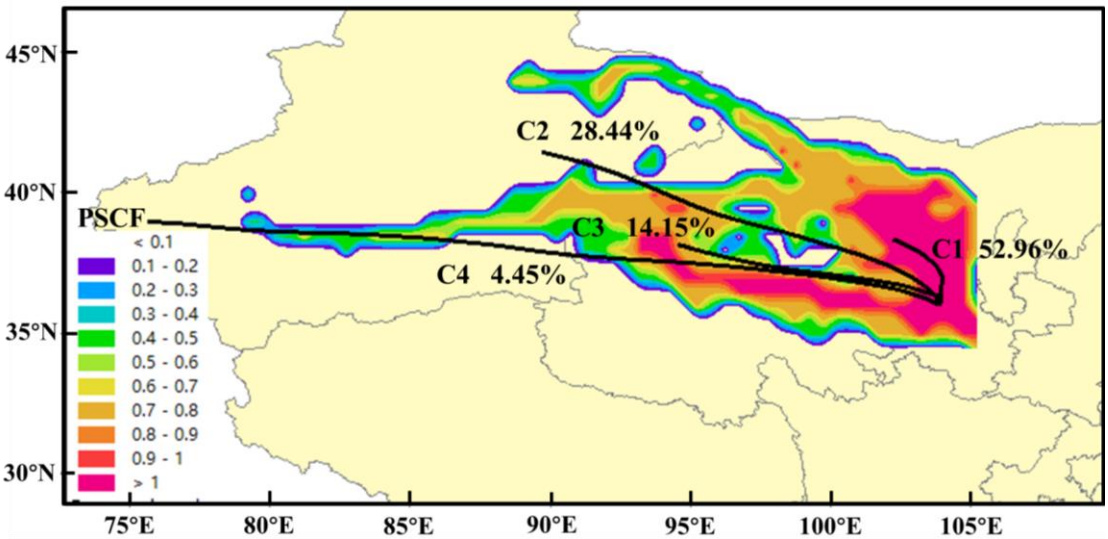

Figure 17. 72-hour backward trajectories and Potential Source Contribution Function (PSCF) values for $PM_{2.5}$ at 100 meters above the Lanzhou Basin floor in January 2021. The black lines represent the clusters of backward trajectories, while the colored shading indicates the magnitude

of the PSCF.

Finally, we highly value the important suggestions you have provided and will make substantial revisions in the introduction, methodology, and results analysis. For example, the combined pollution modeling you suggested, we also have employed both HYSPLIT and footprint model for further analysis. Additionally, we would like to supplement the manuscript with Figure 4 and Figure 17, along with their corresponding analytical results, to further substantiate the conclusions presented in our study.

Specific comments:

1. Page 2, line 6: The term "basin cities" should be clearly defined, along with an explanation of why the analyzed city, Lanzhou, fits this definition. Providing this context is essential for identifying other regions that may experience similar pollution regimes and atmospheric dynamics.

Response: Thank you for your helpful suggestion that we should include a clear definition of "basin city" and explain why Lanzhou fits this definition in the manuscript. We fully agree with you that providing this context is essential for identifying other regions that may experience similar pollution regimes and atmospheric dynamics. The detailed supplementary is as follows.

Basin cities are defined as urban settlements that have developed within basin topographies. These cities typically exhibit several distinctive characteristics: the relative elevation difference between the basin floor and the surrounding mountains or highlands often exceeds 200 meters, the terrain is notably enclosed, and population density tends to be relatively high. Lanzhou, located in a long valley runs mainly from the east to the west with a length of about 30 km, maximum width of 8 km, and depth of 200–600 m (Figure 18), was a typical valley city in a semi-arid region with a population of approximately 4.415 million (Chu et al., 2008; Zhao et al., 2017; Zhao et al., 2019; Zhang et al., 2024).

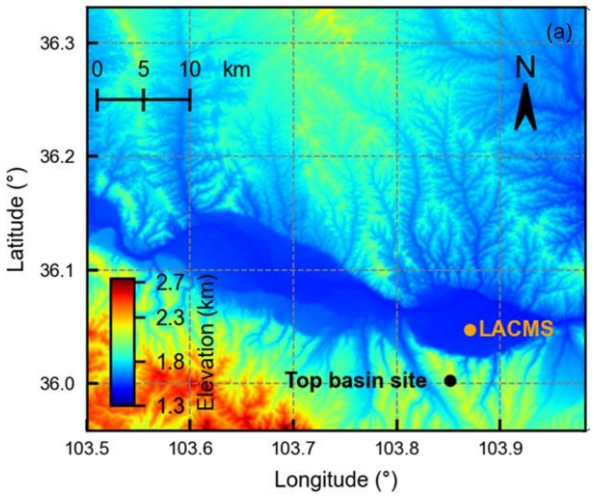

Figure 18. Terrain height (km) near the Lanzhou Basin. (Cited from Zhang et al., 2024, Figure 1a)

2. Page 2, line 17: turbulence is not the only drivers of pollution dispersion. Please check through the manuscript as several oversimplified claims are made.

Response: Thank you for your valuable comment. We have checked through the manuscript and modified it. The modified version is as follows:

Turbulence plays an important role in regulating the transport and mixing of air pollutants within the ABL.

3. Page 3, line 4: UCL is defined in the abstract as urban canopy layer, which justifies the acronym. However here and through the text UCL stands for urban boundary layer, so maybe the acronym should be revised and/or used consistently through the text.

Response: We sincerely thank you for your careful reading and checks. We have modified it.

4. Page 3, line 6 and 8: no need to cite twice Oke, 1987.

Response: We sincerely thank you for your careful reading and constructive comments. We have removed the first “Oke, 1987”.

5. Page 3, line 11-14: this statement is not necessarily always true. More context for such claims is needed.

Response: Thank you for your valuable comment. We have revised the lines 11-14 on page 3 to enhance the objectivity and clarity of our statement more. And the modified version is as follows:

The modified version: Moreover, many kinds of urban construction consume immense amounts of energy, and consumed energy is finally converted to anthropogenic heat, continuously affecting the regional atmosphere (Li et al., 2021). The observational results have portrayed the positive nighttime sensible heat flux in the lower layer (Shi et al., 2019; Zou et al., 2017), indicating the great influences caused by anthropogenic heat in the UCL in winter.

6. Page 5, line 4: it is not clear what the frequency of the observations is. For $PM_{2.5}$ an hourly resolution is mentioned, while for the meteorological/turbulence data no information is provided. Also, the turbulence analyses seem to be done at 30 min resolution, which opens questions about their actual representation of turbulence processes.

Response: Thank you for your careful reading and helpful comment. We are sorry that we did not clarify the details of meteorological and turbulence data in the original manuscript. And, we would like to add the detailed information of the observed elements in the Section 2.1 and present them visually in Table 1.

The Vaisala RS41 radiosondes (Vaisala Oyj Inc., Finland) were launched at 02:00, 08:00, 11:00, 14:00, 17:00, and 20:00 BJT (BJT= UTC + 8 h) from the LACMS. Which observed the meteorological elements profiles of vertical atmospheric column, including wind speed and temperature with a high resolution of 5~7 m. The Micro-Pulse Lidar (MiniMPL, Sigma Space Inc., USA) provided a row backscattered signal at 532 nm with temporal and vertical resolutions of 15 min and 30 m, respectively, and a blind zone of 100 m. And aerosol extinction coefficient profiles were derived using the Fernald method and a simulated annealing algorithm (Fernald, 1984; Press et al., 1993). Observational data are presented in Table 1.

The raw turbulence datasets were sampled at 10 Hz, and pre-processed using Eddy Pro software (Advanced mode, V version 6.2.1, LI-COR Biosciences, Inc., USA). The

pre-processing procedures included exceptional point deletion, error flags, quadratic coordinate rotation, and detrending. Following existed turbulence researches (Foken et al., 2006; Jacobs et al., 2001; Shi et al., 2020), we used 30 min as the average time, which can effectively reduce random errors in turbulence data, capture turbulent characteristics and maintaining statistical reliability. Subsequently, conventional statistical parameters were calculated, including wind speed (WS), wind direction (WD), temperature (T), turbulent kinetic energy (TKE), friction velocity (u_*), and sensible heat flux (H), among others.

Table 1. Detailed description of observation data information.

Site	Date Types	Instruments (Models, Company, and Countries)	Resolution and Accuracy
LACMS 36.05°N, 103.87°E, 1.55 km a.s.l.	Turbulence data Sonic temperature (θ: K), horizontal and vertical velocity components (u, v, w: m s^{-1})	3D-sonic anemometer (CSAT-3B, Campbell Scientific Inc., USA)	10 Hz
	$PM_{2.5}$ (μg m^{-3})	Particulate matter synchronous mixing monitor (5030i SHARP, Thermo Fisher, USA)	1 h
	CO (mg m^{-3})	Online gas analyzer (48i, respectively; Thermo Fisher Scientific, USA)	1 h
	RH (%)	Meteorological sensors (FWE500, FRT, China)	1 h
	Meteorological parameters profiles T (℃), RH (%), WS (m s^{-1}), WD (°)	RS41 Radiosonde (Vaisala Oyj Inc., Finland)	5~7 m 02:00, 08:00, 11:00, 14:00, 17:00 and 20:00
	Profiles of row backscattered signal at 532 nm	Micro Pulse Lidar (Sigma, USA)	bland 100 m 15 min 30 m

7. Page 9, line 20: how is haze defined? Is it just based on pollution concentration?

Response: Thank you for your careful reading and valuable comment. We are sorry that we did not clarify the definition of haze. Therefore, we plan to add the clearer definition in the manuscript. And the detailed supplementary is as follows.

In haze pollution studies, $PM_{2.5}$ is recognized as the primary pollutant. Our study used National Ambient Air Quality Standards (NAAQS) of China (Ministry of Environmental Protection, 2012) to determine haze pollution events, specifically according to the secondary standard threshold (24-hour average $PM_{2.5}$ concentration of 75 μg m^{-3}) since our study area primarily falls under Category II functional zones (urban residential, commercial and industrial areas). Based on this standard, the daily average concentration of $PM_{2.5}$ observed from LACMS exceeded 75 μg m^{-3} on January 2, 12-13, 18, and 20-22, 2021, indicating that air quality reached pollution levels.

8. Page 10, line 2: please rephrase "temperature supposed the development..."

Response: Thank you for your careful reading and helpful suggestion. We have modified it in the manuscript. The modified version is as follows:

Previous studies indicated that higher relative humidity would promote the hygroscopic growth of fine particulate matters (Quan et al., 2011; Chen et al., 2012), while the increase of near-surface temperature would enhance turbulent mixing, thus promoting the development of unstable stratification (Deardorff, 1970; Gao et al., 2016).

9. Page 10, line 10-14: please rephrase, this section is not clear. Also this sentence seems to contradict what was just said above that higher turbulence was present during clear sky periods.

Response: Thank you for your careful reading and constructive comment. We sincerely apologize for the unclear expressions in the original manuscript and we would like to correct them more clearly. The modified version is as follows.

Turbulent kinetic energy (TKE), friction velocity (u_*), sensible heat flux (H) and local atmospheric stability parameter ((z-d)/L) exhibited obvious diurnal variation, with larger absolute values observed from 12:00-18:00 (Figure 19f-19i). Overall, TKE and u_* were higher during the clean periods than the haze pollution periods, whereas H was grater and atmospheric instability was stronger during the pollution period (12:00-18:00). Previous researches have generally found that H in the urban boundary layer was smaller and the atmospheric stratification was more stable during the pollution

periods, which were unfavorable for pollutant dispersion (Ren et al., 2019a; Wang et al., 2020). In contrast, our results demonstrate that within the UCL of basin, atmospheric stratification remained predominantly unstable during pollution periods. This phenomenon might relate to the release of anthropogenic heat and urban canopy storage heat, which is a special phenomenon in UCL of a basin city. In summary, compared to the average turbulent conditions during the clean periods, the dynamic turbulent effect was weaker, while the thermal effect was stronger during the haze pollution periods in the UCL of basin. Both dynamic and thermal turbulence had complied influence on the evolution of haze pollution processes. Next, we would further analyze the specific details of these two pollution cases from the multi-scale turbulence, explore the causes of this pollution pattern in Lanzhou Basin, and how this turbulent transport condition, which was distinguished from most studies, contributed to haze pollution.

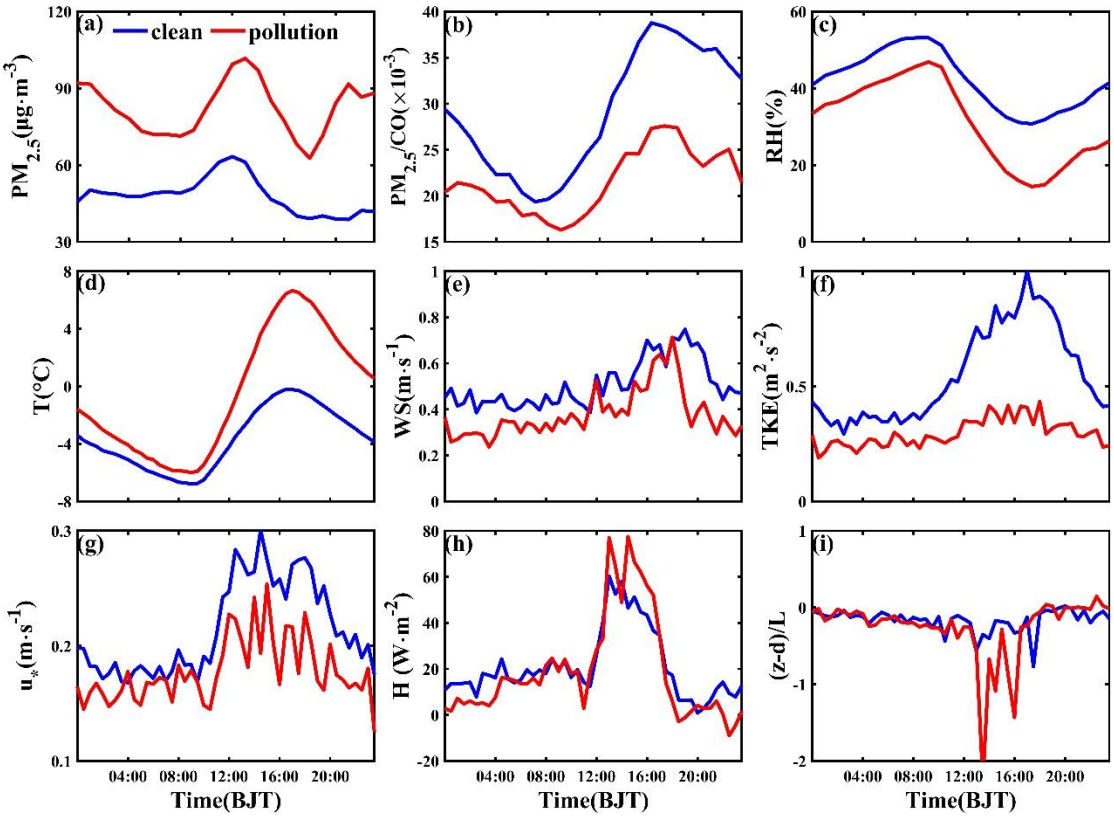

Figure 19. The mean diurnal variation of (a) concentrations of $PM_{2.5}$, (b) $PM_{2.5}$/CO, (c) relative humidity (RH), (d) temperature (T), (e) horizontal wind speed (WS), (f) turbulent kinetic energy (TKE), (g) friction velocity (u_*), (h) sensible heat flux (H), and (i) stability parameter ((z-d)/L) under different conditions from LACMS in January 2021. Solid blue and red lines indicate clean and pollution periods, respectively. (From original manuscript Figure 2)

10. Figure 3: The authors claim that low $PM_{2.5}$ concentrations coincide with TKE peaks. However, it is hard to establish a causal relationship, as similar low $PM_{2.5}$ concentrations are observed through the analyzed events and no TKE peak was observed. Extending the analysis to longer time periods and multiple events may help generalize the conclusions and build more robust statistics. The relationship between TKE and $PM_{2.5}$ can not be based solely on the visual inspection of a time series, such as the one presented in Figure 3.

Response: Thank you for your valuable comment. We sincerely apologize for the vagueness in our original description.

The atmospheric turbulence within the UCL is characterized by strong non-stationarity and inhomogeneity, and these turbulence structures exhibit multi-scale properties (Roman-Cascon et al., 2023). Our focus is on how complex multi-scale turbulent structures in the UCL influence the occurrence and evolution of haze pollution events. And, from the haze pollution cases we analyzed, it can be seen that low $PM_{2.5}$ concentration is related to the value of TKE, ae well as also to the multi-scale turbulent structures that contribute to TKE. The time series relationship between $PM_{2.5}$ concentrations and TKE values is presented in Figure 21 below. It can be observed that low $PM_{2.5}$ concentrations did not exactly coincide with TKE peaks. In detail, multi-resolution decomposition (MRD) analysis further revealed that the small-scale eddies with timescales of less than 2 min contributed significantly to TKE during the strong turbulence period (red box in Figure 20d), whereas during the weak turbulence period (TKE < 1 m^2 s^{-2}), the large-scale eddies with timescales longer than 15 min generally contributed more to TKE. The periods from 14:00 to 18:00 corresponded to the dissipation phase of $PM_{2.5}$, with larger decreases in $PM_{2.5}$ concentrations on January 14th, 19th, and 21st, 2021. The yellow boxes in Figure 20g and Figure 20i showed that the turbulent eddies with timescales shorter than 15 min contributed significantly to TKE. In summary, the contribution of small-scale turbulent eddies with timescales shorter than 2 min to TKE was greater than that of large-scale eddy eddies with timescales longer than 15 min during the pollution periods. From 14:00-18:00, small-scale eddy eddies with timescales shorter than 15 min or even 2 min can efficiently

remove the fine particle matters, resulting in the reduction of $PM_{2.5}$ concentrations.

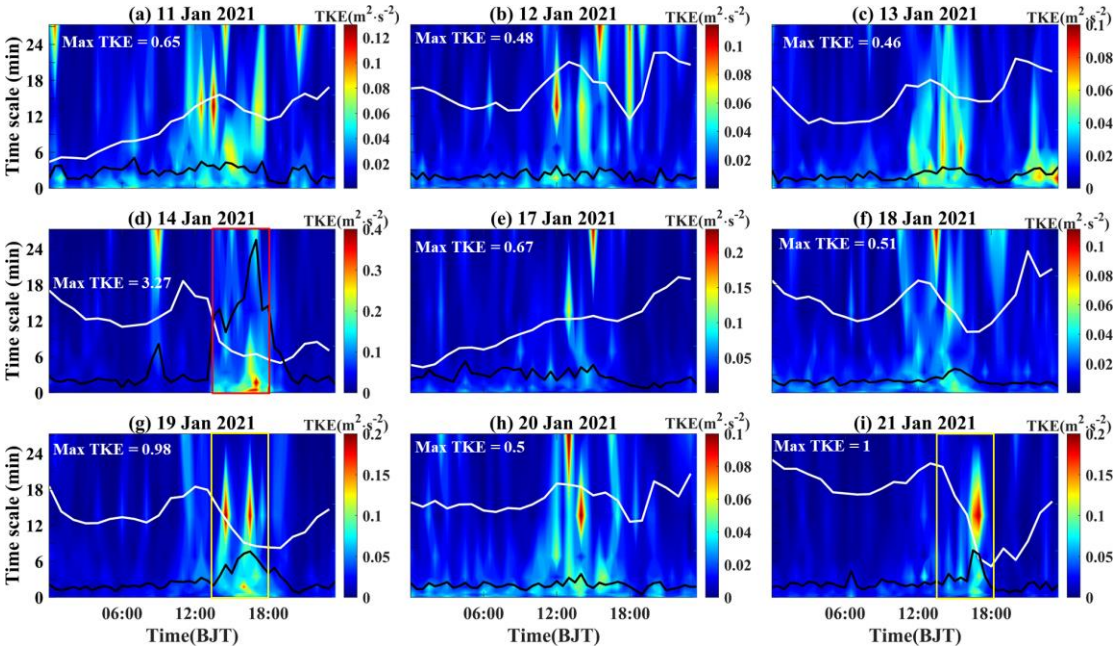

Figure 20. Multi-Resolution Decomposition (MRD) spectra of turbulent kinetic energy (TKE) for Case 1 (January 11–14, 2021, a-d) and Case 2 (January 17–21, 2021, e-i) over 30 min time scales. The solid black and white lines represent TKE average values within 30 min and the $PM_{2.5}$ concentrations, respectively, and the filled colours denote the TKE spectrum values. (From original manuscript Figure 3)

11. Page 13, line 5: Why use KE instead of TKE?

Response: Thank you for your valuable comment.

Our observation platform was located in the UCL, characterized by a highly inhomogeneous distribution of rough elements. Affected by the complex underlying surface of the urban, the collected high-frequency turbulent signals are severely contaminated by sub-mesoscale motions (Anfossi et al., 2005; Vickers and Mahrt, 2006; Mahrt, 2014). In order to quantitatively characterize the sub-mesoscale motions in the original signals, Ren et al. (2019a, 2023a) developed an algorithm based on the Hilbert–Huang transform (HHT) to separate and reconstruct sub-mesoscale and turbulent motions (SMT). And turbulent variable can be separated into two parts by SMT algorithm, that is, $s' = s'_{turb} + s'_{sub}$, represent turbulent motions and sub-mesoscale motions respectively.

TKE represents the turbulent kinetic energy, which is calculated by the original pulsation data. While KE_{turb} denotes the kinetic energy of pure turbulent motions, and

KE_{sub} refers the kinetic energy of sub-mesoscale motions. Additionally, we can calculate the difference in kinetic energy (ΔKE) between the kinetic energy of turbulence and sub-mesoscale motions as well as the local intermittent strength of turbulence (LIST). These detailed parameters can be utilized to further study the impacts of changes in turbulent and sub-mesoscale motions, as well as the influence of turbulence intermittency intensity, on variations in $PM_{2.5}$ concentrations. Detailed calculations are provided below:

$$\mathrm{TKE} = \frac{1}{2}\left(\overline{u'^2} + \overline{v'^2} + \overline{w'^2}\right) \quad (1)$$

$$KE_{turb} = \frac{1}{2}\left(\overline{u'^2_{turb}} + \overline{v'^2_{turb}} + \overline{w'^2_{turb}}\right) \quad (2)$$

$$KE_{sub} = \frac{1}{2}\left(\overline{u'^2_{sub}} + \overline{v'^2_{sub}} + \overline{w'^2_{sub}}\right) \quad (3)$$

$$\Delta\mathrm{KE} = KE_{turb} - KE_{sub} \quad (4)$$

$$LIST = \frac{\sqrt{KE_{turb}}}{\sqrt{KE_{turb}+KE_{sub}}} \quad (5)$$

12. Page 13: the entire page is difficult to follow and more work is needed to generalize mechanisms and findings. Currently results are presented as a series of observations without a clear explanation of what's happening.

Response: Thank you for your valuable comment and suggestion to our study. We have revised this part and further explained the mechanism of energy transition in intermittent turbulence event from the perspective of turbulence fluctuation change with time through a case. The revised version is as follows.

From Figure 21b, 21c, and 21d (yellow arrows), it can be observed that between 08:00 and 13:00, LIST, KE_{turb} and ΔKE were decreasing, while KE_{sub} was increasing. This suggested that the energy of the small-scale mechanical turbulence was dissipating, the influence of the sub-mesoscale motions was relatively increasing, and the value of LIST was decreasing gradually. According to the previous MRD analysis, the large-scale turbulent eddies with timescales longer than 15 min were disturbed by the sub-mesoscale motions. During these periods, the intensity of turbulence intermittency was stronger, coupled with the increase in primary source emission intensity, leading to the

$PM_{2.5}$ concentrations gradually rose. Subsequently, at 14:00-18:00 due to the increase in wind speed and buoyancy, wind shear caused by flow through rough elements and buoyancy convection provided the energy sources. Entering the turbulence burst periods, the turbulence effect gradually intensified (red arrow), with the turbulence intensity reaching maximum, resulting in a corresponding decrease in $PM_{2.5}$ concentrations. At 19:00-22:00 the turbulence intensity weakened and ΔKE rapidly decreased or even ΔKE <0 (green arrow in Figure 21d). Combined with the increase of primary emission, caused $PM_{2.5}$ concentrations rose again.

Ren et al. (2023b) indicated that a sharp reduction of kinetic energy of turbulent contributed to the enhancement of the turbulent barrier effect, and the energy transition of sub-mesoscale to turbulent motions triggered the breaking of turbulent barrier. After ΔKE < 0, the turbulent barrier tended to be broken, followed by a significant increase in ΔKE. In the two haze pollution cases analysed in this study, the wind speed threshold of turbulence intensity ($V_{TKE} = \left[(\frac{1}{2})(\sigma_u^2 + \sigma_v^2 + \sigma_w^2)^{1/2}\right]$) was determined as 0.75 m s^{-1} (Figure 22) according to the method of Sun et al. (2012). At night (19:00-07:00 the next day), the wind speeds were below 0.75 m s^{-1}, and the turbulence intensity was lower, which belonged to regime 1 as Sun et al. (2012) suggested. Intermittency turbulent events were driven by sub-mesoscale motions. At 19:00-22:00 (green arrow in Figure 21d), there was a point where ΔKE < 0, which was quickly followed by a significant increase in ΔKE in the subsequent short period. The phenomenon of energy transfer from sub-mesoscale to turbulence motions occurred, corresponding to the increasing KE_{turb} and decreasing KE_{sub}. Therefore, the horizontal wind speeds and the turbulence intensity at night were lower, while the LIST gradually increased. These short-term turbulent bursts might break the turbulent barrier of the layer and promote the transfer and exchange of substances, which leaded to a decrease in $PM_{2.5}$ concentrations.

We selected an hour period from 23:30 on January 12 to 00:30 on January 13 as a typical case to analyze the intermittent turbulence event. Compared with the previous half hour, the kinetic energy of turbulent motions (KE_{turb}) exhibited a sudden increase

from 00:00 to 00:30 on the 13th, with the average KE_{turb} rising from 0.053 m^2 s^{-2} to 0.448 m^2 s^{-2}. Meanwhile the kinetic energy of sub-mesoscale motions (KE_{sub}) decreased and approached zero (see Figure 23b). This phenomenon corresponded to the burst period in turbulent intermittent event, during which the LIST value began to rise. During the burst period, the mean turbulent momentum fluxes ($-\overline{u'w'}$) increased from about 0.004 m^2 s^{-2} to 0.058 m^2 s^{-2} (see Figure 23a). The synchronous inverse change between the energy of the sub-mesoscale motions and the turbulent motions indicates that the energy transition may occur. Specifically, the energy transition of the sub-mesoscale motions to the turbulent motions drives the short-term turbulence bursts.

During 00:00-07:00 on January 14, 2021, the horizontal wind speeds were lower, LIST, ΔKE and KE_{turb} continuously decreased (blue arrows in Figure 21b, 21c and 21d). This period was in the turbulent quiescent period with high turbulence intermittency intensity, yet it corresponded to a decrease of $PM_{2.5}$ concentration. The scavenging effect of the sub-mesoscale motions required further attention, which would be discussed in the following sections. Overall, turbulence intermittency within the UCL also significantly affected the development of haze pollution, in agreement with other studies in the near-surface layers of urban (Ren et al., 2019a) and relatively flat area (Li et al., 2023).

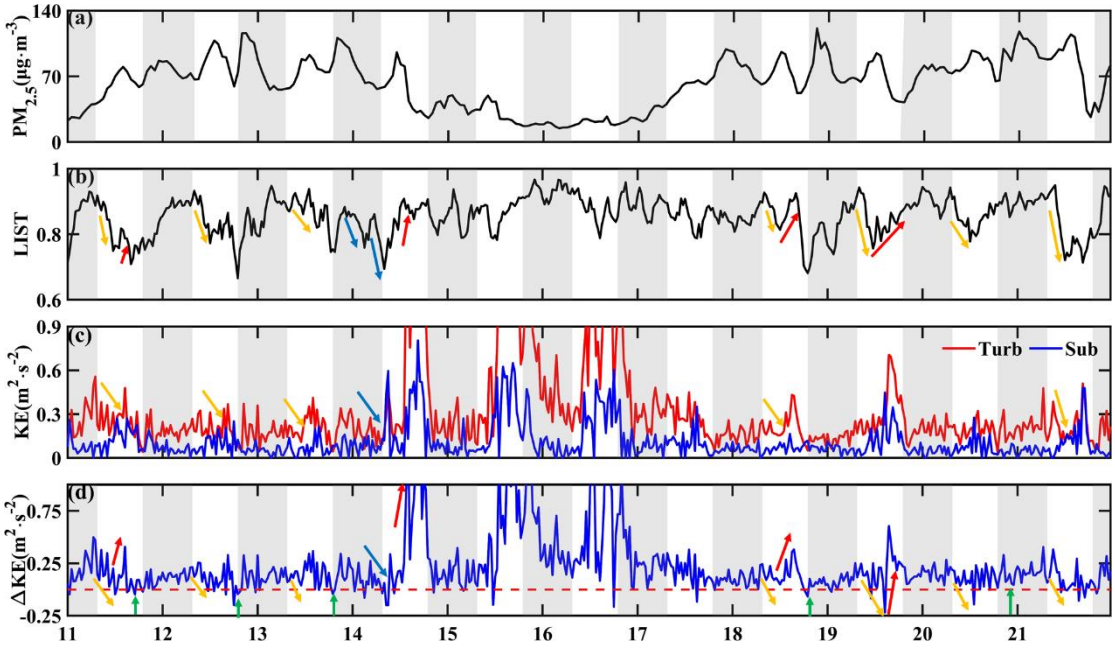

Figure 21. Time series of (a) $PM_{2.5}$ concentration, (b) local intermittent strength of turbulence (LIST), (c) kinetic energy of turbulence (KE_{turb} solid red line) and kinetic energy of sub-mesoscale motion (KE_{sub} solid blue line), and (d) the kinetic energy difference ($\Delta KE = KE_{turb} - KE_{sub}$) from January 11 to 21, 2021. The gray shading represents night between 19:00 and 07:00 the following day. (From original manuscript Figure 4)

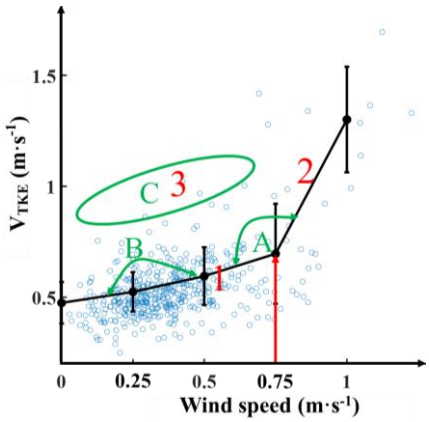

Figure 22. The relationship between turbulence intensity (V_{TKE}) and wind speed, along with three regimes and three types identified of LACMS during January 11–14 and 17–21, 2021, based on the definition by Sun et al. (2012) (From original supplement Figure 2)

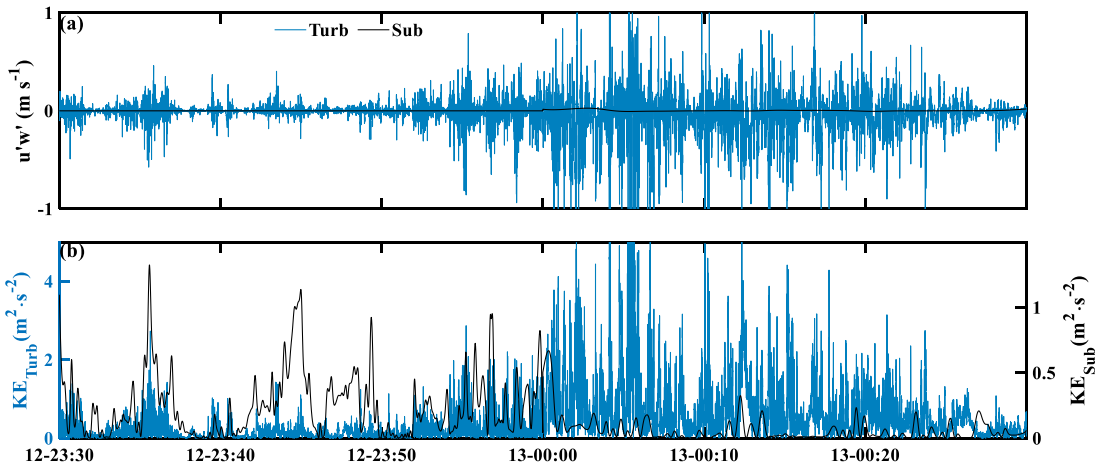

Figure 23. Time series of (a) u′, (b) u′w′, and (c) kinetic energy of turbulent motions (KE_{turb}) and sub-mesoscale motions (KE_{sub}) from January 11 to 21, 2021 From 23:30 on January12, 2021, to 00:30 on January 13, 2021.

13. Figure 4: what are the yellow and green arrows?

Response: Thank you for your valuable comment. We sincerely apologize for not clearly articulating the meanings of the different colors of arrows in Figure 4 of the original manuscript. We intend to describe clearly the meaning of these arrows in the manuscript.

In Figure 21b-21d of original manuscript, downward trends indicated by yellow

arrows are observed, representing the gradual intensification of turbulence intermittency from 08:00 to 13:00. This suggests that the energy of turbulent motions was dissipating, while the influence of sub-mesoscale motions was relatively increasing. Numerical results show that LIST, KE_{turb}, and KE decrease, whereas KE_{sub} increases. Several green arrows in Figure 21d indicate that ΔKE gradually decreases and even falls below zero between 19:00 and 22:00. Following this, a significant short-term increase in ΔKE corresponds to a decline in $PM_{2.5}$ concentrations. During these processes, the kinetic energy of turbulence (KE_{turb}) continues to rise, while the kinetic energy of sub-mesoscale motions (KE_{sub}) diminishes, indicating an energy transfer from sub-mesoscale to turbulent motions. These short-term turbulent bursts might break the turbulent barrier of the layer and promote the transfer and exchange of substances, which leaded to a decrease in $PM_{2.5}$ concentrations.

Finally, the detailed analysis and case-specific illustrations will be added to the main text. Figure 23 here will also be included in the supplementary figures for readers to examine the details.

14. Figure 5 and quadrant analysis: this section needs to be revised as it's not clear what the key outcome of this analysis is and how conclusions are supported/drawn.

Response: Thank you for your valuable comments to our study. We are sincerely sorry that we did not clearly state the key outcome of the analysis and how the conclusions were supported. Therefore, we have made the following revises to this section.

Although the development of turbulent vortices in the UCL was constrained by rough elements, thermal turbulence might still have some coherent structures that affected the transport and diffusion of fine particulate matters. We further utilized the quadrant analysis to examine the influence turbulent coherent structures within the UCL on the momentum fluxes and sensible heat fluxes transport. The turbulent coherent structures mainly consist of ejections and sweeps (Li and Bou-Zeid, 2011), and different topology of turbulent coherent structures can be identified based on the characteristics of the difference in the flux contribution and time fraction of ejections and sweeps.

The downgradient transport of momentum fluxes predominantly occurred from

14:00-18:00 (shaded gray in Figure 24b and 24h), with the sweeps (quadrant 4, solid green line) dominating the transport of momentum fluxes, whereas the outward interactions and inward interactions motions (quadrants 1 and 3, solid black and blue lines) dominated the counter-gradient transport of momentum fluxes in most of the other time periods. For the sensible heat flux (Figure 24c and 24i), during the clean periods (such as January 15th), the ejections and sweeps (quadrants 1 and 3, solid black and blue lines) dominated throughout most of the day, presenting $\overline{w'\theta'} > 0$. Only occasionally at night or early morning, presenting $\overline{w'\theta'} < 0$. the ejections and sweeps (quadrants 2 and 4, solid red and green lines) dominated or four quadrants contributed equally. The phenomenon of $\overline{w'\theta'} < 0$ occurred occasionally during the night or early morning, characterized by the dominance of ejections and sweeps (quadrants 2 and 4, indicated by solid red and green lines) or by equal contributions from all four quadrants. While during polluted periods, this situation ($\overline{w'\theta'} < 0$) was more common at night or early morning, because stable boundary layer was more likely to occur at night or early morning when there was pollution. However, the phenomenon of $\overline{w'\theta'} > 0$ still dominated during the daytime. In summary, the presence of the UCL disrupted the downward transport of momentum, and the release outward from the urban heat storage during the night time likely resulted in a positive sensible heat flux, which are consistent with other studies (Zou et al., 2017; Shi et al., 2019).

The coherent structures of turbulent contributed significantly to the development of the boundary layer above UCL and the pollutants transport. As shown by the gray shadow in Figure 24c and 24i the flux contributions of ejections (quadrant 1, solid black line) were greater than sweeps (quadrant 3, solid blue line) from 10:00 to 13:00, while the time fraction (see Figure 24d and 24j) of ejections (quadrant 1, solid black line) were smaller than sweeps (quadrant 3, solid blue line). That was, less but intense updrafts surrounded by numerous but weak downdrafts, which was well consistent with the behaviour of thermal plumes (Stull, 1988). Maitani and Ohtaki (1987) pointed out that the ejections are more efficient than sweeps in transporting heat under unstable conditions. The presence of thermal plumes during pollution periods was slightly more than during clean periods, which enhanced the transportation efficiency of sensible heat

flux. That further explained why the sensible heat flux was greater between 12:00 and 18:00 during the pollution periods. In addition, the effective transport of sensible heat flux by the thermal plumes promoted the elevation of the atmospheric boundary layer in the afternoon. As shown in the temperature profiles (Figure 25a and 25c), the temperature inversion layer weakened or disappeared between 11:00 and 17:00, and the fine particulate matters could further diffuse upward into the atmosphere. It was also evident that the aerosol extinction coefficient was higher at the same height during the pollution period (10:00 to 13:00), with the extinction coefficient profiles showing an "up-convex" shape (Figure 24a and 24g). In this study, the concentration of fine particulate matters generally decreased with height (Figure 24a and 24g). At 14:00-18:00, sweeps simultaneously transferred momentum flux and sensible heat flux, and also transported cleaner air from the upper part of the canopy downward to the interior of UCL. During this period, the turbulence intensity in the UCL was high, leading to clean air transported downward mix with the fine particulate matters, thus reducing the $PM_{2.5}$ concentrations in the near-surface. Similarly, it can be seen from Figure 24a and 24g that the peak value of extinction coefficient profiles gradually decreased during 14:00-18:00. However, the extinction coefficient contour at 14:00-18:00 on January 13, 2021 (white box) showed a peak at 400 m and a break at 200 m above the ground. Further analysis of the wind speed profiles during this period revealed that the wind speeds below 500 m were less than 1 m s^{-1} (Figure 25b), indicating weak diffusion and limiting the vertical extent of the sweeps effect.

In addition to the coherent structure formed by turbulent motions, sub-mesoscale motions could also exhibit organization and coherence. The previous analysis indicated that the turbulent eddies within the UCL were broken and susceptible to the influence of sub-mesoscale motions, which could trigger turbulent intermittency events under the weak turbulent conditions. These sub-mesoscale motions also form organized coherent structures that affect the pollution processes. Analogous to the analysis method for coherent structures in turbulence, Figure 24e and 24k display the correlation coefficient R_{sub} for the sub-mesoscale motions, and Figure 24f and 24l display the flux contribution difference ΔS for the sub-mesoscale motions. Section 3.2 discussed the analysis of

turbulence intermittency from 00:00 to 07:00 on January 14, 2021, where strong turbulence intermittency and weak turbulence intensity were observed, but this period was associated with a decrease in $PM_{2.5}$ concentrations. From Figure 24e and 24f, R_{sub} and $\Delta S > 0$ (gray shading) during 00:00 to 07:00 on January 14, 2021, indicated that the sub-mesoscale motions in this period were dominated by downward motion (i.e., $w'_{sub} < 0$ and $u'_{sub} < 0$). When $w'_{sub} < 0$ and $u'_{sub} < 0$, the relatively clean air outside the UCL or the upper basin was transported downward, which diluted the fine particle matters in the UCL. As shown in the aerosol extinction coefficient profiles (red arrow in Figure 24a), the zero-contour line of the extinction coefficient gradually extended to the lower part of basin over time from 00:00 to 07:00 on January 14, 2021. Although the turbulence intermittency was strong and the turbulent diffusion ability was weak at this time, the organized structure formed by the larger-scale sub-mesoscale motions played a positive role in the dissipation of $PM_{2.5}$. In other pollution periods, the coherence of sub-mesoscale motions was also greater than 0 between 23:00 and to 07:00 the next day. Despite weak dynamic turbulence intermittency during this time, these organized sub-mesoscale motions might also have contributed to $PM_{2.5}$ removal. For example, when $w'_{sub} > 0$ and $u'_{sub} > 0$ (gray shadows on January 12th in Figure 24f, 18th and 20th in Figure 24l), $PM_{2.5}$ with higher concentration in the UCL was transported upward and subsequently removed more easily with the help of stronger airflow above the canopy, resulting in a decrease in $PM_{2.5}$ concentrations.

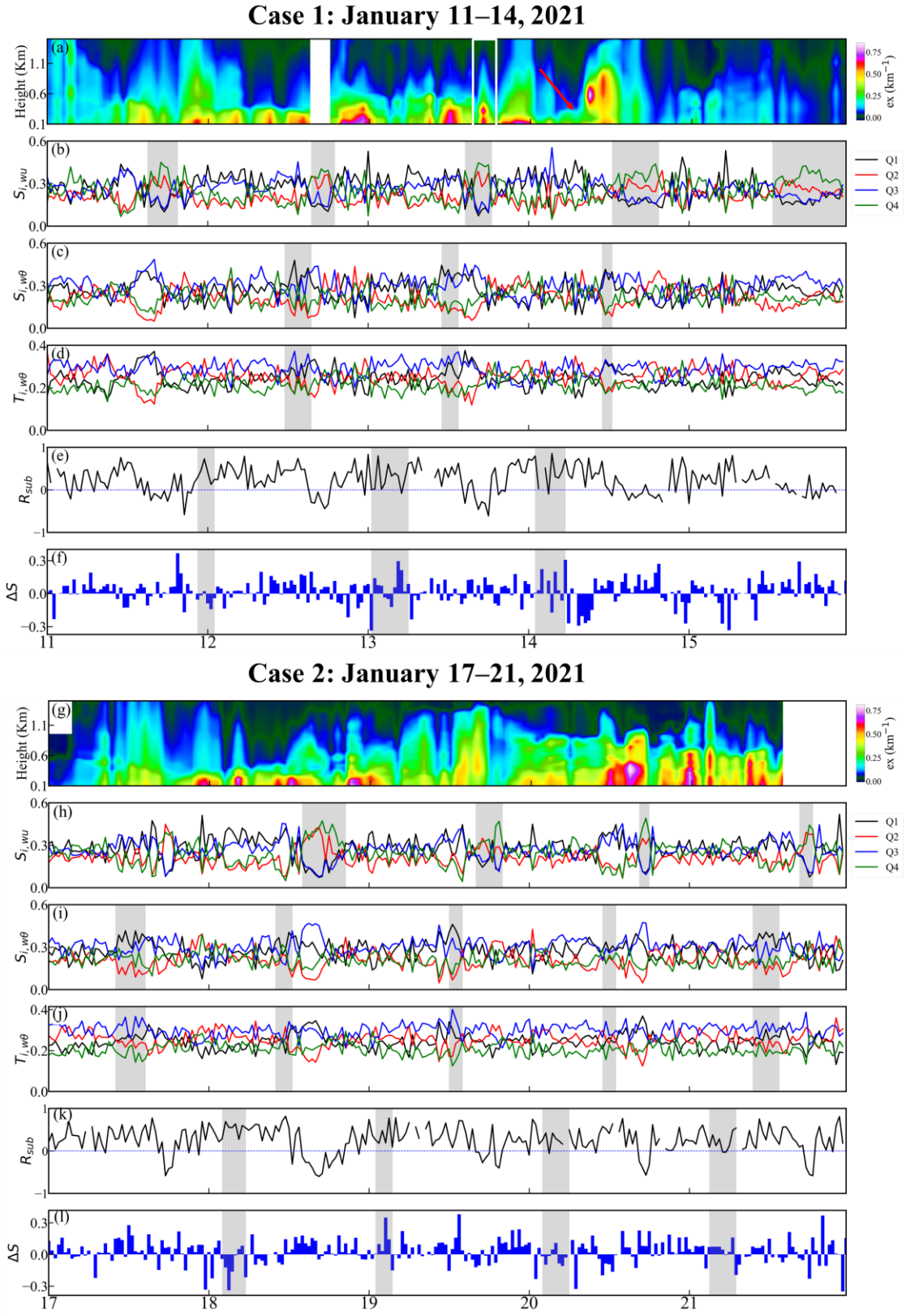

Figure 24. Time series of (a,g) aerosol extinction coefficient profiles, (b,h) flux contribution of each quadrant for momentum, (c,i) flux contribution of each quadrant for sensible heat, (d,j) time fraction of each quadrant for sensible heat flux, (e,k) correlation coefficient of sub-mesoscale

motions (R_{sub}), (f,l) flux contribution of sub-mesoscale difference between the downward and upward motion (ΔS) from January 11–15, 2021, (top panels) and January 17–21, 2021, (bottom panels). The solid black, red, blue, and green lines represent the results of the quadrants 1, 2, 3, and 4, respectively. (From original manuscript Figure 5)

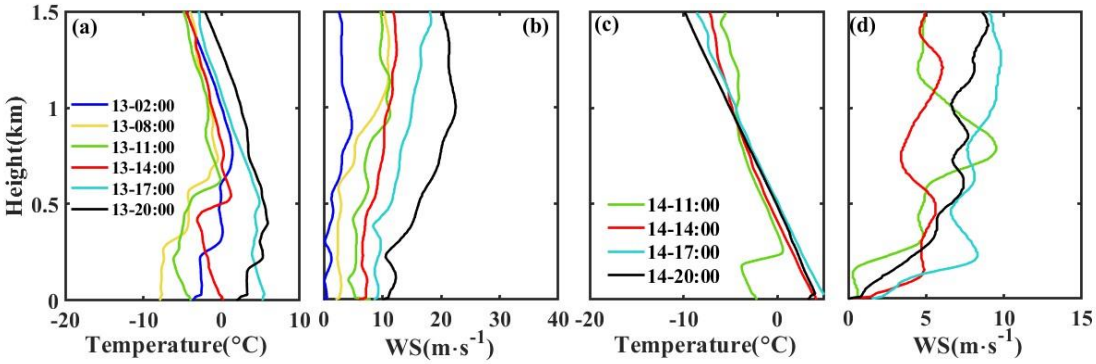

Figure 25. Temperature (a, c) and wind speed (b, d) profiles of LACMS on January 13 (a, b) and January 14 (c, d), 2021. Since wind speeds were low throughout January 13, a successive 2 m s^{-1} offset was applied to each wind speed profile to enhance visual distinction (no offset for the first profile, accumulating to +10 m s^{-1} for the sixth) (From original supplement Figure 3)

15. Page 18: from the title of section 3.4 and through the manuscript it is not very clear where the multi-scale component of turbulence comes from, how it is diagnosed and what is causing that.

Response: Thank you for your valuable and constructive comments to our study. We sincerely apologize for the vagueness about the multi-scale component of turbulence in section 3.4 of original manuscript. Therefore, we would like to introduce the characteristics of turbulent and sub-mesoscale motions in the spectra and the basis for partitioning them. We also mark the position of the spectral gap with dotted lines in the spectra and further explain the causes of multi-scale component of turbulence.

Based on traditional turbulence theory, the turbulent energy spectrum can generally be divided into three regions: the energy-containing vortex region, the inertial subregion, and the dissipation region, as shown in Figure 26. Van der Hoven (1957) presented an analysis on the large spectrum of horizontal wind speeds, which showed a notable spectral gap of approximately 1 cycle h^{-1} between the macroscale (synoptic) and microscale (turbulent) parts of the spectrum (see Figure 27). Many other studies have generally proven the existence of the spectral gap (Panofsky, 1969; Fiedler and

Panofsky, 1970).

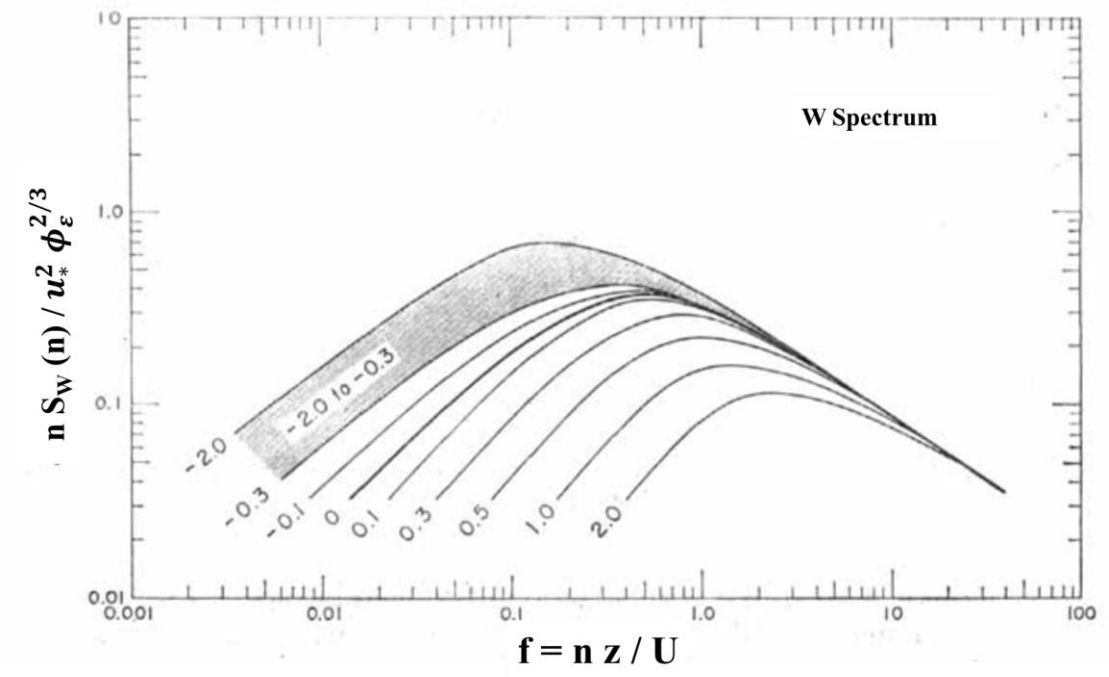

Figure 26. Generalized w spectrum for z/L values ranging from +2.0 to -2.0. (Cited from Kaimal et al., 1972, Figure 4)

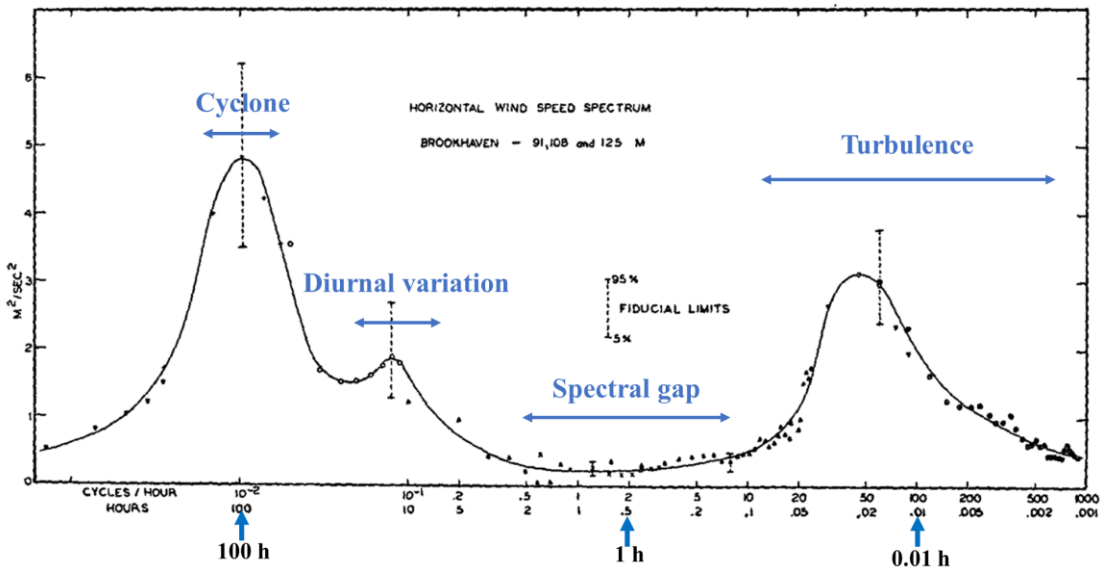

Figure 27. Horizontal wind-speed spectrum at Brookhaven National Laboratory at about 100-m height. (Cited from Van der Hoven., 1957, Figure 1)

To decompose turbulent and sub-mesoscale parts in the observed fluctuations, spectral approaches are usually adopted, on the basis of the appearance of spectral gaps between turbulence and sub-mesoscale motions (Mahrt, 2007; Wei et al. 2017; Mahrt and Bouzeid, 2020). Common spectral analysis methods include wavelet analysis

(Salmond 2005), multi-resolution decomposition (MRD; Vickers and Mahrt 2003; Acevedo et al. 2014) and Hilbert–Huang transform (HHT; Huang et al. 2008; Wei et al. 2017), where the latter appears to be superior since it is fully data driven. Ren et al. (2019a) developed an algorithm based on the HHT to separate and reconstruct sub-mesoscale and turbulent motions (SMT). The proposed algorithm looks for spectral gaps between large- (weather-scale) and small-scale (turbulence-scale) motions from the Hilbert spectra of observational data, based on which the algorithm subsequently reconstructs the turbulent motion series. In the second-order Hilbert spectra (see Figure 13), the significant spectral gaps were clearly visible. The right sides of these spectral gaps aligned with the expectations of classical energy spectrum theory, whereas the left sides showed deviations from these expectations. Analogously, we can clearly observe the significant spectral gaps in the energy spectra observed in the UCL (see dotted blue lines in Figure 28a1-28d1). The right sides of these spectral gaps aligned with the expectations of classical energy spectrum theory, while the left sides showed deviations.

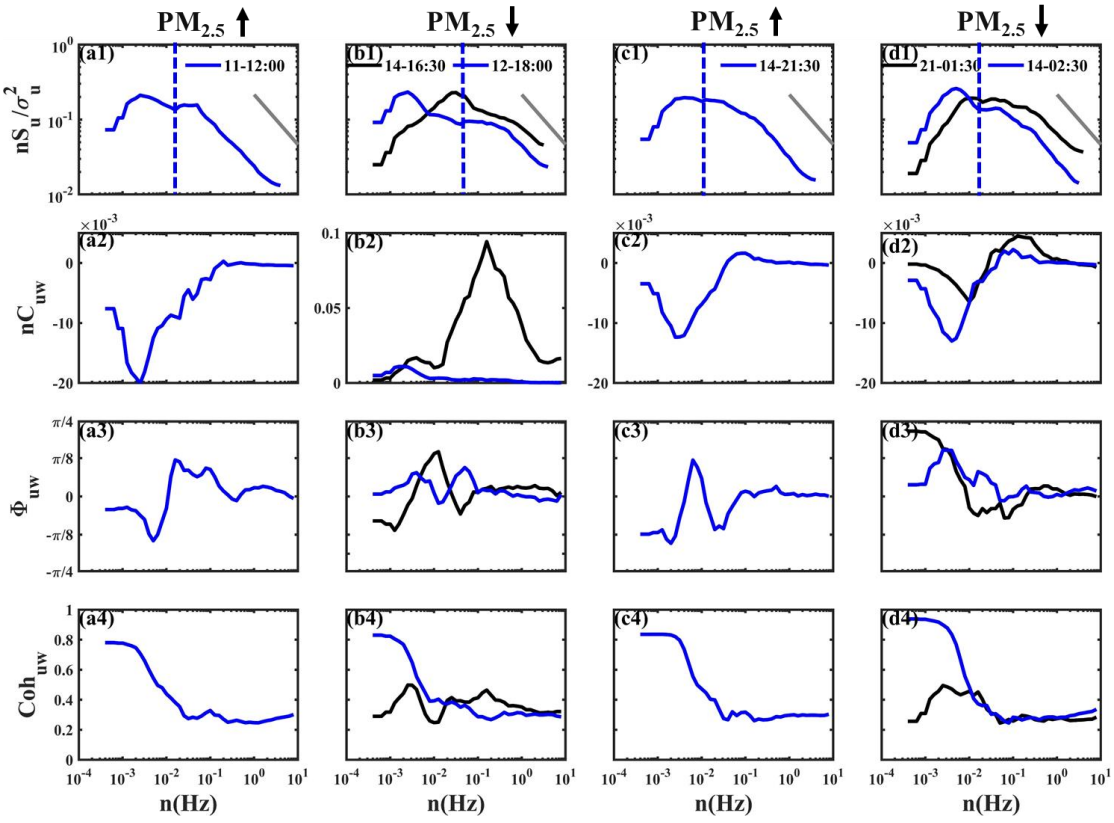

Figure 28. (a1–d1) Energy spectra of u, the dashed blue lines represent the spectral gaps between the sub-mesoscale motions and the turbulent motions, the solid gray lines represent the slope of -2/3; (a2–d2) covariance spectra of uw; (a3–d3) phase spectra of uw; and (a4–d4) coherence

spectra of uw within the UCL of basin. Six time points were selected to represent the following: (a1-a4) 12:00 on the January 11, 2021, (b1-b4) 16:30 on the January 14, 2021 (solid black line) and 18:00 on the January 12, 2021 (solid blue line); (c1-c4) 21:30 on the January 14, 2021, (d1-d4) 01:30 on the January 21, 2021 (solid black line) and 02:30 on the January 14, 2021 (solid blue line). (From original manuscript Figure 6)

The urban boundary layer consists of the urban near-surface layer and the outer layer, among which the UCL represents the atmosphere close to the ground layer below the top of urban buildings (Oke et al., 2017). UCL is the most drastically affected by pollution sources emissions from surface and anthropogenic activities. The distribution of rough elements (e.g., buildings, trees) within the UCL is highly inhomogeneous in three-dimensional space, and the development of turbulent eddies can easily be restricted or fragmented by the influence of rough elements. Moreover, many kinds of urban construction consume immense amounts of energy, and consumed energy is finally converted to anthropogenic heat, continuously affecting the regional atmosphere (Li et al., 2021). Consequently, atmospheric turbulence within the UCL is characterized by strong non-stationarity and inhomogeneity. These turbulence structures exhibit multi-scale properties (Román-Cascón et al., 2023) that may be influenced by sub-mesoscale motions (Ren et al., 2019a). Multiple observational studies have demonstrated that sub-mesoscale motions are site dependent and tend to be greater in complex terrain (Anfossi et al., 2005; Vickers and Mahrt, 2007; Wei et al., 2021; Zhang et al., 2024). Mahrt (2014) also mentioned that although sub-mesoscale motions seem to always be present, their impact is limited primarily to weak-wind conditions. Therefore, our study observed sub-mesoscale motions under the same conditions described in reported studies: complex terrains and weak winds. The observed non-turbulent motions of "dirty wave" (see Figure 5) in high-frequency fluctuations also match existing studies (Zhang et al., 2024).

16. Figure 6: why are only 6 time points considered? Why not examine more complete statistics?

Response: Thank you for your valuable comment and helpful suggestion.

The contribution of the turbulence spectra varies across different time scales for each 30-min segment. When averaging is performed, certain features, such as the frequency corresponding to the peak of the turbulence spectra and the position of the spectral gaps, may be distorted. To address this, we selected 6 representative time points with typical characteristics to illustrate four stages of haze pollution pattern: $PM_{2.5}$ concentrations rose from 08:00-13:00, declined from 14:00-18:00, rose again from 19:00-21:00, and declined from 22:00-07:00 the next day. In addition to the 6 time points, there are other time points whose turbulence spectra also align with the corresponding characteristics. Therefore, we added these other time points in Figure 6 of the original manuscript and presented consistent results (see Figure 29).

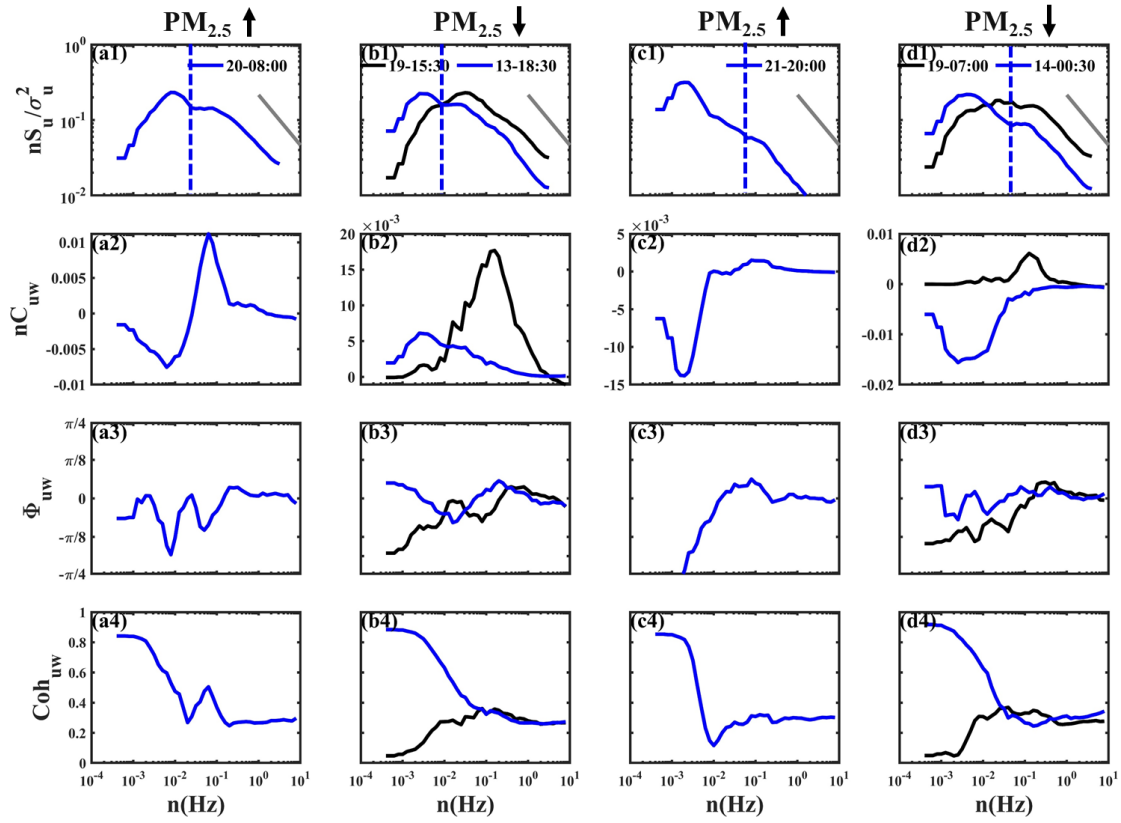

Figure 29. as same as Figure 28. Another six time points were selected to represent the following: (a1-a4) 08:00 on the January 20, 2021, (b1-b4) 15:30 on the January 19, 2021 (solid black line) and 18:30 on the January 13, 2021 (solid blue line); (c1-c4) 20:00 on the January 21, 2021, (d1-d4) 07:00 on the January 19, 2021 (solid black line) and 00:30 on the January 14, 2021 (solid blue line).

17. Page 20, line 9: the paper does not address any urban related process as there is no spatial component/variability in the observations analyzed. It is therefore

challenging to attribute the findings presented to urban scale processes. The conclusions should be revised accordingly in multiple instances.

Response: Thank you for your valuable and helpful comments and suggestions. We have made some supplementary adjustments and modifications based on your suggestions, which helped to enhance the reliability and objectivity of our study conclusions. The details are as follows.

We fully agree that observational data from a single monitoring station may not adequately capture spatial variations in turbulence and pollution dynamics across the city. Based on this, we conducted a station average analysis of $PM_{2.5}$ concentration data from other 4 state-controlled monitoring sites of Lanzhou Basin city in January 2021. Then, we compared the results with those from the observation station (LACMS) in the original manuscript, and found that their pattern characteristics were consistent. Furthermore, we have similarly analyzed the $PM_{2.5}$ concentration data from subsequent observations conducted from December 2023 to February 2024, and the results have also shown consistency (see Figure 2). In summary, the spatial and temporal characteristics Lanzhou Basin city from January 2021 and December 2023 to February 2024 exhibit consistency. Thank you again for your constructive suggestions, which increase the reliability of our study conclusions on the spatio-temporal characteristics of haze pollution pattern.

The turbulence data observed by the eddy covariance system, affected by the highly inhomogeneous distribution of rough elements, primarily reflect the region dominated by the characteristics of roughness elements around the site. This scale is generally considered the street scale (see Figure 3). Although rough elements in the UCL exhibit varying distribution characteristics across different regions, their presence exerts certain common effects on dynamic and thermal turbulence. For example, significant roughness caused by the canopy and its geometry directly influences the flow fields (Russell et al., 2016; Zou et al., 2017; Shi et al., 2023), and the anthropogenic heat and urban canopy storage heat will continuously affect the regional atmosphere (Li et al., 2021). Existing studies examining the correlation between turbulence and air pollution are mainly based on single monitoring station (Wang et

al.,2020; Shi et al., 2023; Román-Cascón et al., 2023). Unfortunately, due to a lack of encrypted turbulence observations in Lanzhou Basin city at present, we are unable to obtain additional turbulence data from that location. However, we can provide extended observation records from our monitoring sites, which further substantiate the generality of our results. For specific conclusions regarding this matter, please refer to the third reply in the General comments.

Finally, thanks again for your valuable comments. We would like to standardize the terminology related to the study scale (urban microscale meteorological) and supplement the analysis of spatio-temporal coherence of the pollution and the turbulence analysis of longer time series in the UCL of Lanzhou Basin city in section 3.1. Which would help enhance reliability and objectivity of our conclusions.

References

Acevedo, O. C., Costa, F. D., Oliveira, P. E. S., Puhales, F. S., Degrazia, G. A., and Roberti, D. R.: The influence of submeso processes on stable boundary layer similarity relationships, J. Atmos. Sci., 71, 207–225, https://doi.org/10.1175/JAS-D-13-0131.1, 2014.

Acevedo, O. C., and Fitzjarrald, D. R.: The influence of submeso processes on stable boundary layer similarity relationships, J. Atmos. Sci., 71, 207–225, https://doi.org/10.1175/JAS-D-13-0131.1, 2014.

Ahmad, K., Khare, M., and Chaudhry, K. K.: Wind tunnel simulation studies on dispersion at urban street canyons and intersections—a review, J. Wind Eng. Ind. Aerodyn., 93, 697–717, https://doi.org/10.1016/j.jweia.2005.04.003, 2005.

Allouche, M., Bou-Zeid, E., Ansorge, C., Katul, G. G., Chamecki, M., Acevedo, O., Thanekar, S., and Fuentes, J. D.: The detection, genesis, and modeling of turbulence intermittency in the stable atmospheric surface layer, J. Atmos. Sci., 79, 1171–1190, https://doi.org/10.1175/JAS-D-21-0053.1, 2022.

Anfossi, D., Oetti, D., Degrazia, G., and Boulart, A.: An analysis of sonic anemometer observations in low wind speed conditions, Bound.-Layer Meteorol., 114, 179–203, https://doi.org/10.1007/s10546-004-1984-4, 2005.

Cava, D., Giostra, U., and Katul, G.: Characteristics of gravity waves over an Antarctic ice sheet during an austral summer, Atmosphere, 6, 1271–1289, https://doi.org/10.3390/atmos6091271, 2015.

Chang, H., Ren, Y., Zhang, H., Liang, J., Cao, X., Tian, P., Li, J., Bi, J., and Zhang, L.: The characteristics of turbulence intermittency and its impact on surface energy imbalance over Loess Plateau, Agric. Forest. Meteorol., 354, 110088, https://doi.org/10.1016/j.agrformet.2024.110088, 2024.

Chen, J., Zhao, C. S., Ma, N., Liu, P. F., Göbel, T., Hallbauer, E., Deng, Z. Z., Ran, L., Xu, W. Y., Liang, Z., Liu, H. J., Yan, P., Zhou, X. J., and Wiedensohler, A.: A parameterization of low visibilities for hazy days in the North China Plain, Atmos. Chem. Phys., 12, 4935–4950, https://doi.org/10.5194/acp-12-4935-2012, 2012.

Chu, P. C., Chen, Y. C., Lu, S. H., Li, Z. C., and Lu, Y. Q.: Particulate air pollution in Lanzhou China, Environ. Int., 34, 698–713, https://doi.org/10.1016/j.envint.2008.01.006, 2008.

Coulter, R. L., and Doran, J. C.: Spatial and temporal occurrences of intermittent turbulence during CASES-99, Bound.-Layer Meteorol., 105, 329–349, https://doi.org/10.1023/A:1019993703820, 2002.

Deardorff, J. W.: Convective Velocity and Temperature Scales for the Unstable Planetary Boundary Layer and for Rayleigh Convection, J. Atmos. Sci., 27, 1211–1213, https://doi.org/10.1175/1520-0469(1970)027<1211:CVATSF>2.0.CO;2, 1970.

Deb Burman, P. K. D., Prabha, T. V., Morrison, R., and Karipot, A.: A case study of turbulence in the nocturnal boundary layer during the Indian summer monsoon, Bound.-Layer Meteorol., 169, 115–138, https://doi.org/10.1007/s10546-018-0364-4, 2018.

Doran, J. C.: Characteristics of intermittent turbulent temperature fluxes in stable conditions, Bound.-Layer Meteorol., 112, 241–255, https://doi.org/10.1023/B:BOUN.0000027907.06649.d0, 2004.

Draxler, R. R., and Rolph, G. D.: Hybrid single-particle Lagrangian integrated trajectory (HYSPLIT) Model, NOAA Air Resour. Lab. Silver Spring, MD, 2003.

Durden, D. J.: On the impact of wave-like disturbances on turbulent fluxes and turbulence statistics in nighttime conditions: a case study, Biogeosciences, 10, 8433–8443, https://doi.org/10.5194/bg-10-8433-2013, 2013.

Fernald, F. G.: Analysis of atmospheric lidar observations some comments, Appl. Opt., 23, 652–653, https://doi.org/10.1364/AO.23.000652, 1984.

Fiedler, F., and Panofsky, H. A.: Atmospheric Scales and Spectral Gaps, B. Am. Meteorol. Soc., 51, 1114–1120, https://doi.org/10.1175/1520-0477(1970)051<1114:ASASG>2.0.CO;2, 1970.

Foken, T., Wimmer, F., Mauder, M., Thomas, C., and Liebethal, C.: Some aspects of the energy balance closure problem, Atmos. Chem. Phys., 6, 4395–4402, https://doi.org/10.5194/acp-6-4395-2006, 2006.

Gao, Z., Liu, H., Russell, E. S., Huang, J., Foken, T., and Oncley, S. P.: Large eddies modulating flux convergence and divergence in a disturbed unstable atmospheric surface layer, J. Geophys. Res. Atmos., 121, 1475–1492, https://doi.org/10.1002/2015JD024529, 2016.

Hang, J., and Chen, G.: Experimental study of urban microclimate on scaled street canyons with various aspect ratios, Urban Clim., 46, 101299, https://doi.org/10.1016/j.uclim.2022.101299, 2022.

Huang, Y. X., Schmitt, F. G., Lu, Z. M., and Liu, Y. L.: An amplitude-frequency study of turbulent scaling intermittency using empirical mode decomposition and Hilbert spectral analysis, Europhys. Lett., 84, 40010, https://doi.org/10.1209/0295-5075/84/40010, 2008.

Jacobs, A. F., van de Wiel, B. J., and Holtslag, A. A.: Daily course of skewness and kurtosis within and above a crop canopy, Agric. Forest. Meteorol., 110, 71–84, https://doi.org/10.1016/S0168-1923(01)00284-8, 2001.

Jia, W. X., Zhang, X. Y., Zhang, H. S., and Ren, Y.: Turbulent transport dissimilarities of particles, momentum, and heat, Environ. Res., 211, 113111, https://doi.org/10.1016/j.envres.2022.113111, 2022.

Ju, T. T., Wu, B. G., Zhang, H. S., Wang, Z. Y., and Liu, J. L.: Impacts of boundary-layer structure and turbulence on the variations of $PM_{2.5}$ during Fog-Haze episodes,

Bound.-Layer Meteorol., 183, 469–493, https://doi.org/10.1007/s10546-022-00691-z, 2022.

Kaimal, J. C., and Finnigan, J. J.: Atmospheric boundary layer flows: Their structure and measurements, Oxford Univ. Press, 1994.

Kaimal, J. C., Wyngaard, J. C., Izumi, Y., and Coté, O. R.: Spectral characteristics of surface-layer turbulence, Q. J. Roy. Meteor. Soc., 98, 563–589, https://doi.org/10.1002/qj.49709841707, 1972.

Katul, G. G., Albertson, J., and Parlange, M.: Conditional sampling, bursting, and the intermittent structure of sensible heat flux, J. Geophys. Res. Atmos., 99, 22869–22876, https://doi.org/10.1029/94JD01679, 1994.

Katul, G., Kuhn, G., Schieldge, J., and Hsieh, C. I.: The ejection-sweep character of scalar fluxes in the unstable surface layer, Bound.-Layer Meteorol., 83, 1–26, https://doi.org/10.1023/A:1000293516830, 1997.

Kljun, N., Calanca, P., Rotach, M. W., and Schmid, H. P.: A simple two-dimensional parameterisation for Flux Footprint Prediction (FFP), Geosci. Model Dev., 8, 3695–3713, https://doi.org/10.5194/gmd-8-3695-2015, 2015.

Lareau, N. P., Crosman, E., Whiteman, C. D., Horel, J. D., Hoch, S. W., Brown, W. O. J., and Horst, T. W.: The persistent cold-air pool study, B. Am. Meteorol. Soc., 94, 51–63, https://doi.org/10.1175/BAMS-D-11-00255.1, 2013.

Li, D., and Bou-Zeid, E.: Coherent structures and the dissimilarity of turbulent transport of momentum and scalars in the unstable atmospheric surface layer, Bound.-Layer Meteorol., 140, 243–262, https://doi.org/10.1007/s10546-011-9613-5, 2011.

Li, L., Chan, P. W., Deng, T., Yang, H. L., Luo, H. Y., Xia, D., and He, Y. Q.: Review of advances in urban climate study in the Guangdong-Hong Kong-Macau Greater Bay Area, China, Atmos. Res., 261, 105759, https://doi.org/10.1016/j.atmosres.2021.105759, 2021.

Li, Q. H., Zhang, H. S., Zhang, X. Y., Cai, X. H., Jin, X. P., Zhang, L., Song, Y., Kang, L., Hu, F., and Zhu, T.: COATS: comprehensive observation on the atmospheric boundary layer three-dimensional structure during haze pollution in the North China Plain, Sci. China Earth Sci., 66, 939–958, https://doi.org/10.1007/s11430-

022-1092-y, 2023.

Liu, C., Yang, Q., Shupe, M. D., Ren, Y., Peng, S., Han, B., and Chen, D.: Atmospheric turbulent intermittency over the Arctic Sea-ice surface during the MOSAiC expedition, J. Geophys. Res. Atmos., 128, e2022JD038790, https://doi.org/10.1029/2023JD038639, 2023.

Mahrt, L.: Nocturnal boundary-layer regimes, Bound.-Layer Meteorol., 88, 255–278, https://doi.org/10.1023/A:1001171313493, 1998.

Mahrt, L.: Weak-wind mesoscale meandering in the nocturnal boundary layer, Environ. Fluid Mech., 7, 331–347, https://doi.org/10.1007/s10652-007-9024-9, 2007.

Mahrt, L.: Stably stratified atmospheric boundary layers, Annu. Rev. Fluid Mech., 46, 23–45, https://doi.org/10.1146/annurev-fluid-010313-141354, 2014.

Mahrt, L., and Bou-Zeid, E.: Non-stationary boundary layers, Bound.-Layer Meteorol., 177, 189–204, https://doi.org/10.1007/s10546-020-00533-w, 2020.

Maitani, T., and Ohtaki, E.: Turbulent transport processes of momentum and sensible heat in the surface layer over a paddy field, Bound.-Layer Meteorol., 40, 283–293, https://doi.org/10.1007/BF00117452, 1987.

Ministry of Environmental Protection, China.: Ambient Air Quality Standards (GB 3095-2012), 655, http://www.wxbh.gov.cn/doc/2021/11/04/3479116.shtml, 2012.

Mo, Z., and Liu, C. H.: Inertial and roughness sublayer flows over real urban morphology: A comparison of wind tunnel experiment and large-eddy simulation, Urban Clim., 49, 101530, https://doi.org/10.1016/j.uclim.2023.101530, 2023.

Muschinski, A., Frehlich, R. G., and Balsley, B. B.: Small-scale and large-scale intermittency in the nocturnal boundary layer and the residual layer, J. Fluid Mech., 515, 319–351, https://doi.org/10.1017/S0022112004000412, 2004.

Oke, T. R., Mills, G., Christen, A., and Voogt, J. A.: Urban Climates, Cambridge Univ. Press, 525 pp, https://doi.org/10.1017/9781139016476, 2017.

Panofsky, H. A.: Spectra of atmospheric variables in the boundary layer, Radio Sci., 4, 1101–1109, https://doi.org/10.1029/RS004i012p01101, 1969.

Press, W. H., Teukolsky, S. A., Vettering, W. T., and Flannery, B. R.: Numerical Recipes in Fortran: The Art of Scientific Computing, Cambridge Univ. Press, New York,

1993.

Quan, J., Zhang, Q., He, H., Liu, J., Huang, M., and Jin, H.: Analysis of the formation of fog and haze in North China Plain (NCP), Atmos. Chem. Phys., 11, 8205–8214, https://doi.org/10.5194/acp-11-8205-2011, 2011.

Raupach, M. R., Thom, A. S., and Edwards, I.: A wind-tunnel study of turbulent flow close to regularly arrayed rough surfaces, Bound.-Layer Meteorol., 18, 373–397, https://doi.org/10.1007/BF00120968, 1980.

Ren, Y., Zhang, H. S., Wei, W., Wu, B. G., Cai, X. H., and Song, Y.: Effects of turbulence structure and urbanization on the heavy haze pollution process, Atmos. Chem. Phys., 19, 1041–1057, https://doi.org/10.5194/acp-19-1041-2019, 2019a.

Ren, Y., Zhang, H. S., Wei, W., Wu, B. G., and Liu, J. L.: Comparison of the turbulence structure during light and heavy haze pollution episodes, Atmos. Res., 230, 104645, https://doi.org/10.1016/j.atmosres.2019.104645, 2019b.

Ren, Y., Zhang, H. S., Zhang, L., and Liang, J. N.: Quantitative description and characteristics of submeso motion and turbulence intermittency, Q. J. Roy. Meteor. Soc., 149, 1726–1744, https://doi.org/10.1002/qj.4479, 2023a.

Ren, Y., Zhang, H. S., Wu B. G., Zhang, L., Liang, J. N., and Zhang, X. Y.: Energy transition in the enhancement and break of turbulence barrier during heavy haze pollution, Environ. Pollut., 317, 120770, https://doi.org/10.1016/j.envpol.2022.120770, 2023b.

Ren, Y., Zhang, H. S., Zhang, X. Y., Cai, X. H., Song, Y., Liang, J. N., Zhang, L., Zhu, T., and Huang, J. P.: Research progress and current application of weak turbulence and turbulence intermittency in stable boundary layers, Earth-Sci. Rev., 262, 105062, https://doi.org/10.1016/j.earscirev.2025.105062, 2025.

Román-Cascón, C., Yagüe, C., Ortiz-Corral, P., Serrano, E., Sánchez, B., Sastre, M., Maqueda, G., Alonso-Blanco, E., Artiñano, B., Gómez-Moreno, F. J., Diaz-Ramiro, E., Fernández, J., Martilli, A., García, A. M., Núñez, A., Cordero, J. M., Narros, A., and Borge, R.: Wind and turbulence relationship with NO~2~ in an urban environment: a fine-scale observational analysis, Urban Clim., 51, 101663, https://doi.org/10.1016/j.uclim.2023.101663, 2023.

Román-Cascón, C., Yagüe, C., Mahrt, L., Sastre, M., Steeneveld, G. J., Pardyjak, E., van de Boer, A., and Hartogensis, O.: Interactions among drainage flows, gravity waves and turbulence: a BLLAST case study, Atmos. Chem. Phys., 15, 9031–9047, https://doi.org/10.5194/acp-15-9031-2015, 2015.

Rotach, M., Vogt, R., Bernhofer, C., et al.: BUBBLE — an Urban Boundary Layer Meteorology Project, Theor. Appl. Climatol., 81, 231–261, https://doi.org/10.1007/s00704-004-0117-9, 2005.

Roth, M.: Review of atmospheric turbulence over cities, Q. J. Roy. Meteor. Soc., 126, 941–990, https://doi.org/10.1002/qj.49712656409, 2000.

Roth, M., and Oke, T. R.: Turbulent transfer relationships over an urban surface. I. Spectral characteristics, Q. J. Roy. Meteor. Soc., 119, 1071–1104, https://doi.org/10.1002/qj.49711951311, 1993.

Russell, E. S., Liu, H. P., Gao, Z. M., Lamb, B., and Wagenbrenner, N.: Turbulence dependence on winds and stability in a weak-wind canopy sublayer over complex terrain, J. Geophys. Res. Atmos., 121, 11502–11515, https://doi.org/10.1002/2016JD025057, 2016.

Salmond, J. A.: Wavelet analysis of intermittent turbulence in a very stable nocturnal boundary layer: Implications for the vertical mixing of ozone, Bound.-Layer Meteorol., 114, 463–488, https://doi.org/10.1007/s10546-004-2422-3, 2005.

Shah, S. K., and Bou-Zeid, E.: Direct numerical simulations of turbulent Ekman layers with increasing static stability: Modifications to the bulk structure and second-order statistics, J. Fluid Mech., 760, 494–539, https://doi.org/10.1017/jfm.2014.588, 2014.

Shi, Y., and Hu, F.: Ramp-like $PM_{2.5}$ accumulation process and z-less similarity in the stable boundary layer, Geophys. Res. Lett., 47, e2019GL086530, https://doi.org/10.1029/2019GL086530, 2020.

Shi, Y., Hu, F., Fan, G. Q., and Zhang, Z.: Multiple technical observations of the atmospheric boundary layer structure of a red-alert haze episode in Beijing, Atmos. Meas. Tech., 12, 4887–4901, https://doi.org/10.5194/amt-12-4887-2019, 2019.

Shi, Y., Zeng, Q. C., Hu, F., Ding, W. C., Zhang, Z., Zhang, K., and Liu, L.: Different

turbulent regimes and vertical turbulence structures of the urban nocturnal stable boundary layer, Adv. Atmos. Sci., 40, 1089–1103, https://doi.org/10.1007/s00376-022-2198-8, 2023.

Shi, Y., Zeng, Q. C., Liu, L., Cheng, X. L., and Hu, F.: Important role of turbulent wind gust and its coherent structure in the rapid removal of urban air pollution, Environ. Res. Commun., 4, 075001, https://doi.org/10.1088/2515-7620/ac7c5f, 2022.

Stull, R. B.: An Introduction to Boundary Layer Meteorology, Springer, 670 pp, https://doi.org/10.1007/978-94-009-3027-8, 1988.

Sun, J. L., Mahrt, L., Banta, R. M., and Pichugina, Y. L.: Turbulence regimes and turbulence intermittency in the stable boundary layer during CASES-99, J. Atmos. Sci., 69, 338–351, https://doi.org/10.1175/JAS-D-11-082.1, 2012.

Van der Hoven, I.: Power Spectrum of Horizontal Wind Speed in the Frequency Range from 0.0007 to 900 Cycles Per Hour, J. Atmos. Sci., 14, 160–164, https://doi.org/10.1175/1520-0469(1957)014<0160:PSOHWS>2.0.CO;2, 1957.

Van der Linden, S. J. A., Van de Wiel, B. J. H., Petenko, I., Van Heerwaarden, C. C., Baas, P., and Jonker, H. J. J.: A Businger mechanism for intermittent bursting in the stable boundary layer, J. Atmos. Sci., 77, 1–48, https://doi.org/10.1175/JAS-D-19-0309.1, 2020.

Vercauteren, N., Boyko, V., Kaiser, A., Belušić, D., and Grisogono, B.: Statistical investigation of flow structures in different regimes of the stable boundary layer, Bound.-Layer Meteorol., 173, 143 – 164, https://doi.org/10.1007/s10546-019-00464-1, 2019.

Vickers, D., and Mahrt, L.: The cospectral gap and turbulent flux calculations, J. Atmos. Ocean. Tech., 20, 660–672, https://doi.org/10.1175/1520-0426(2003)20<660:TCGATF>2.0.CO;2, 2003.

Vickers, D., and Mahrt, L.: A solution for flux contamination by mesoscale motions with very weak turbulence, Bound.-Layer Meteorol., 118, 431–447, https://doi.org/10.1007/s10546-005-9003-y, 2006.

Wang, L. L., Fan, S. H., Hu, F., Miao, S. G., Yang, A. Q., Li, Y. B., Liu, J. K., Liu, C. W., Chen, S. S., Ho, H. C., Duan, Z. X., Gao, Z. Q., and Yang, Y. J.: Vertical

gradient variations in radiation budget and heat fluxes in the urban boundary layer: a comparison study between polluted and clean air episodes in Beijing during winter, J. Geophys. Res. Atmos., 125, e2020JD032478, https://doi.org/10.1029/2020JD032478, 2020.

Wang, Y. Q.: MeteoInfo: GIS software for meteorological data visualization and analysis, Meteorol. Appl., 21, 360–368, https://doi.org/10.1002/met.1345, 2014.

Wei, W., Schmitt, F. G., Huang, X. Y., and Zhang, H. S.: The analyses of turbulence characteristics in the atmospheric surface layer using arbitrary-order Hilbert spectra, Bound.-Layer Meteorol., 159, 391–406, https://doi.org/10.1007/s10546-015-0122-9, 2016.

Wei, W., Zhang, H. S., Schmitt, F. G., Huang, Y. X., Cai, X. H., Song, Y., Huang, X., and Zhang, H.: Investigation of turbulence behaviour in the stable boundary layer using arbitrary-order Hilbert spectra, Bound.-Layer Meteorol., 163, 311–326, https://doi.org/10.1007/s10546-016-0227-9, 2017.

Wei, Z. R., Zhang, L., Ren, Y., Wei, W., Zhang, H. S., Cai, X. H., Song, Y., and Kang, L.: Characteristics of the turbulence intermittency and its influence on the turbulent transport in the semi-arid region of the Loess Plateau, Atmos. Res., 249, 105312, https://doi.org/10.1016/j.atmosres.2020.105312, 2021.

Xu, J., Shi, J., Zhang, Q., Ge, X., Canonaco, F., Prévôt, A. S. H., Vonwiller, M., Szidat, S., Ge, J., Ma, J., An, Y., Kang, S., and Qin, D.: Wintertime organic and inorganic aerosols in Lanzhou, China: sources, processes, and comparison with the results during summer, Atmos. Chem. Phys., 16, 14937–14957, https://doi.org/10.5194/acp-16-14937-2016, 2016.

Zhang, L., Zhang, H. S., Cai, X., Song, Y., and Zhang, X.: Characteristics of Turbulence Intermittency, Fine Structure, and Flux Correction in the Taklimakan Desert, J. Atmos. Sci., 81, 459–475, https://doi.org/10.1175/JAS-D-23-0107.1, 2024.

Zhang, L., Zhang, H. S., Li, Q., Cai, X., and Song, Y.: Vertical dispersion mechanism of long-range transported dust in Beijing: effect of atmospheric turbulence, Atmos. Res., 269, 106033, https://doi.org/10.1016/j.atmosres.2022.106033, 2022.

Zhang, M., Tian, P. F., Zhao, Y. Y., Song, X., Liang, J. N., Li, J. Y., Zhang, Z. D., Guan,

X., Cao, X. J., Ren, Y., Shi, J. S., and Zhang, L.: Impact of aerosol-boundary layer interactions on PM~2.5~ pollution during cold air pool events in a semi-arid urban basin, Sci. Total Environ., 922, 171225, https://doi.org/10.1016/j.scitotenv.2024.171225, 2024.

Zhao, S., P., Yu, Y., Qin, D., Yin, D., and He, J.: Assessment of long-term and large-scale even-odd license plate controlled plan effects on urban air quality and its implication, Atmos. Environ., 170, 82–95, https://doi.org/10.1016/j.atmosenv.2017.09.041, 2017.

Zhao, S., P., Yu, Y., Qin, D., Yin, D., Du, Z., Li, J., Dong, L., He, J., and Li, P.: Measurements of submicron particles vertical profiles by means of topographic relief in a typical valley city, China, Atmos. Environ., 199, 102–113, https://doi.org/10.1016/j.atmosenv.2018.11.035, 2019.

Zou, J., Zhou, B. W., and Sun, J. N.: Impact of eddy characteristics on turbulent heat and momentum fluxes in the urban roughness sublayer, Bound.-Layer Meteorol., 164, 39–62, https://doi.org/10.1007/s10546-017-0244-3, 2017.

Zou, J., Sun, J. N., Liu, G., Yuan, R. M., and Zhang, H. S.: Vertical Variation of the Effects of Atmospheric Stability on Turbulence Statistics Within the Roughness Sublayer Over Real Urban Canopy, J. Geophys. Res. Atmos., 123, 2017–2036. https://doi.org/ 10.1002/2017JD027041, 2018